were flushed with normal saline. Using a dissection microscope, colon tumors were noted grossly for their location, number, and diameter, and measured with calipers. All tumors from AOM-treated C57BL/6J mice were subjected to histological examination after routine processing and H&E staining. The remaining small intestinal mucosa was removed by scraping and used for AMPK measurement. High-density lipoprotein cholesterol was assessed by FUJI DRI-CHEM4000 (FUJIFILM Medical Co., Ltd., Tokyo, Japan). Total body fat amount was determined by EchoMRI-100 (Echo Medical Systems, Houston, TX).

AOM-Induced Colon Aberrant Crypt Foci Development in APN-Deficient Mice Treated With Pai-1 Blocker

Male $APN^{-/-}$ C57BL/6J mice (n = 10 each) of 6 weeks in age received AOM at a dose of 10 mg/kg body weight intraperitoneally once a week for 3 weeks. From the first treatment with AOM, mice were fed control AIN-76A or experimental diet containing Pai-1 blocker SK-216,[11] chemically synthesized at Shizuoka Coffein Co. Ltd., at 50 and 100 ppm for 8 weeks. All mice were sacrificed 5 weeks after the first dose of AOM. After laparotomy, the entire colons were resected, fixed, stained with 0.2% methylene blue and scored for the number of aberrant crypt foci (ACF)/colon according to the procedure of previous report.[16]

Experimental Protocol for Min *Mice Treated With Metformin*

To investigate the effects of AMPK activation on Pai-1 expression levels, four male *Min* mice at 6 weeks of age were given 1000 ppm metformin, 1,1-dimethylbiguanide hydrochloride (Wako Chemical, Osaka, Japan) in the diet for 14 weeks and liver samples were collected. Control group mice were fed basal diet without metformin.

Detection of Intestinal Phosphorylated AMPK Levels

The concentrations of p-AMPK in the small intestine (n = 4) and colon (n = 4) from 9-week-old male $APN^{+/+}$, $APN^{+/-}$, and $APN^{-/-}$ C57BL/6J mice, and in the liver (n = 4) from 12-week-old male $APN^{+/+}$ *Min*, $APN^{+/-}$ *Min*, and $APN^{-/-}$*Min* mice were determined using an AMPKα [pT172] enzyme-linked immunosorbent assay kit (Invitrogen, Carlsbad, CA), according to the manufacturer's protocol. Concentrations of p-Akt and total Akt in the small intestine were determined using a PathScan Cell Growth 4-Plex Array Kit (Cell Signaling Technology, Inc., Danvers, MA) for 6 samples from 55-week-old male $APN^{+/+}$, $APN^{+/-}$, and $APN^{-/-}$ C57BL/6J mice, according to the manufacturer's protocol.

Real-Time PCR Analysis and Reverse Transcription PCR Analysis

Tissue samples from livers of male *Min* mice with $APN^{+/+}$, $APN^{+/-}$, and $APN^{-/-}$ genotypes and C57BL/6J mice with $APN^{+/+}$, $APN^{+/-}$, and $APN^{-/-}$ genotypes were used. Total RNA was isolated from tissues using Isogen (Nippon Gene, Tokyo, Japan), treated with DNase I (Invitrogen) and 3 μg aliquots in a final volume of 20 μL were used for synthesis of complementary DNA using an Omniscript RT Kit (Qiagen, Hilden, Germany) and an oligo(dT) primer. Primers for mouse Adipo-R1, mouse Adipo-R2, and glyceraldehyde-3-phosphate dehydrogenase were employed as reported previously.[17] Cycling conditions were as follows: 94°C for 5 seconds, annealing temperature (60–66°C) for 30 seconds, 72°C for 60 seconds, and 32 cycles after an initial step of 95°C for 3 minutes. A final elongation step of 72°C for 10 minutes completed the PCR. The products were then electrophoresed on 2% agarose gels. Real-time PCR was carried out using a DNA Engine Opticon TM 2 (MJ Japan Ltd., Tokyo, Japan) with SYBR Green Real-time PCR Master Mix (Toyobo Co., Osaka, Japan) according to the manufacturer's instructions. Primers for mouse Pai-1, mouse casein kinase 2β (CK2β), and glyceraldehyde-3-phosphate dehydrogenase were employed as reported previously.[18,19] To assess the specificity of each primer set, amplicons generated from the PCR reaction were analyzed for melting curves and also by electrophoresis in 2% agarose gels.

Determination of Serum Adipocytokine Levels

The concentrations of APN in the plasma were determined using a Quantikine Adiponectin/Acrp30 Immunoassay Kit (R&D Systems, Inc., Minneapolis, MN). Total of 4 or 5 samples from 12-week-old male *Min* mice with $APN^{+/+}$, $APN^{+/-}$, and $APN^{-/-}$ genotypes and 10 samples from 55-week-old C57BL/6J mice with $APN^{+/+}$, $APN^{+/-}$, and $APN^{-/-}$ genotypes, were treated according to manufacturer's protocol. Pai-1, leptin, resistin, TNFα, interleukin (IL)-6, and monocyte chemotactic protein-1 (MCP-1) were measured using Multiplex kits (LINCOplex, St Louis, MO).

Primary Cultures of APN*-Deficient Fibroblast Cells and Treatment With Insulin or IL-6*

Primary cultures of fibroblasts were prepared from newborn $APN^{-/-}$ and $APN^{+/+}$ C57BL/6J mouse epidermis after separation from the dermis by a trypsin flotation method.[20] Cells were maintained in Dulbecco's modified Eagle's medium supplemented with 10% heat-inactivated fetal bovine serum (Hyclone Laboratories, Inc., Logan, UT) at 37°C in 5% CO_2. Fibroblasts were plated in 24-well cell culture dishes at a density of 100,000 cells/dish, with Dulbecco's modified Eagle's medium containing 10% fetal bovine serum. After 12 hours

culture without FBS, 1 μg/mL insulin (Invitrogen) or 50 ng/mL IL-6 (R&D Systems) was added in the medium for 5 or 10 minutes. After treatment, the fibroblasts were lysed in 100 μL lysis buffer (0.0625 M Tris-HCl [pH 6.8], 20% 2-mercaptoethanol, 10% glycerol, 5% sodium dodecyl sulfate) with Halt phosphatase inhibitor cocktail (Pierce Biotechnology, Rockford, IL) and Complete Mini, protease inhibitor cocktail tablets (Roche Diagnostics, Mannheim, Germany). Samples were separated in 10% polyacrylamide gel electrophoresis-sodium dodecyl sulfate gels and transferred onto polyvinylidene difluoride membranes (Millipore, Billerica, MA). Antibodies against the p-Akt (Ser473), p-Erk1/2 (Thr202/Thy204; Cell Signaling Technology), and β-actin (Biomedical Technologies Inc, Stoughton, MA) were used at a 2000× dilution. Antibodies against the Bcl-2 (Santa Cruz Biotechnology, CA) were used at a 200× dilution. Peroxidase-conjugated secondary antibodies for anti-rabbit IgG were obtained from GE Healthcare, Buckinghamshire, UK. Blots were developed with enhanced chemoluminescence (ECL) (GE Healthcare). Protein levels were evaluated by detecting the density of the band using NIH Image 1.62, and the data normalized by the density of β-actin.

Immunohistochemical Staining

Colon with tumors from 55-week-old male C57BL/6J mice of $APN^{+/+}$, $APN^{+/-}$, and $APN^{-/-}$ genotypes (n = 6 each) and the middle segments of the small intestines of 9-week-old male *Min* mice of $APN^{+/+}$, $APN^{+/-}$, and $APN^{-/-}$ genotypes (n = 6 each) were prepared for immunohistochemical examination using polyclonal rabbit anti-receptor for activated protein C kinase 1 (RACK1) antibody (Santa Cruz Biotechnology) and monoclonal mouse anti-CK2β antibody (Pierce Biotechnology) at 100× dilution. As the secondary antibody, biotinylated anti-rabbit IgG and anti-mouse IgG (Vector Laboratories, Burlingame, CA) were employed at a 200× dilution. Staining was performed using avidin-biotin reagents (Vectastain ABC reagents; Vector Laboratories), 3,3′-diaminobenzidine, hydrogen peroxide, and hematoxylin. As a negative control, consecutive sections were immunostained without exposure to the primary antibody.

Statistical Analysis

The significance of differences in the incidences of AOM-induced mouse tumors was analyzed using the χ^2 test and other statistical analyses were performed with the Dunnett's multiple comparison test. Statistical significance was concluded with P values $<.05$.

Results

Generation of APN-Deficient Min *Mice*

To determine the effect of the deficiency of APN on intestinal polyp formation in *Min* mice, we introduced a knockout mutation of the *APN* gene into the *Min* mice by successive cross-mating and generated *Min* mice that carried $APN^{+/-}$ and $APN^{-/-}$ mutations. The quantity of serum APN observed in $APN^{+/+}$*Min* mice, 5.6 μg/mL, was decreased by almost half in $APN^{+/-}$*Min* mice, 3.0 μg/mL, and none was detected in $APN^{-/-}$*Min* mice (Figure 1*A*). APN receptors, Adio-R1 and -R2, were clearly observed, and both expression levels were not affected by APN deficiency (Figure 1*B*). Genotyping did not significantly affect food intake, behavior, or body weight changes during the experimental periods. Final body weights in the 12-week-old male $APN^{+/+}$*Min*, $APN^{+/-}$*Min*, and $APN^{-/-}$*Min* mice were 25.5 ± 1.6, 24.9 ± 1.3 and 23.8 ± 3.0 g, respectively, and in female mice were 20.6 ± 1.7, 20.5 ± 1.5, and 20.1 ± 0.6 g.

An age-dependent change of serum TG levels was observed in $APN^{+/+}$*Min* mice fed basal diet at 9 and 12 weeks of age, the levels rising from 53 to 143 mg/dL in males (Supplementary Figure). Comparing serum levels of TG in APN-deficient male *Min* mice with male

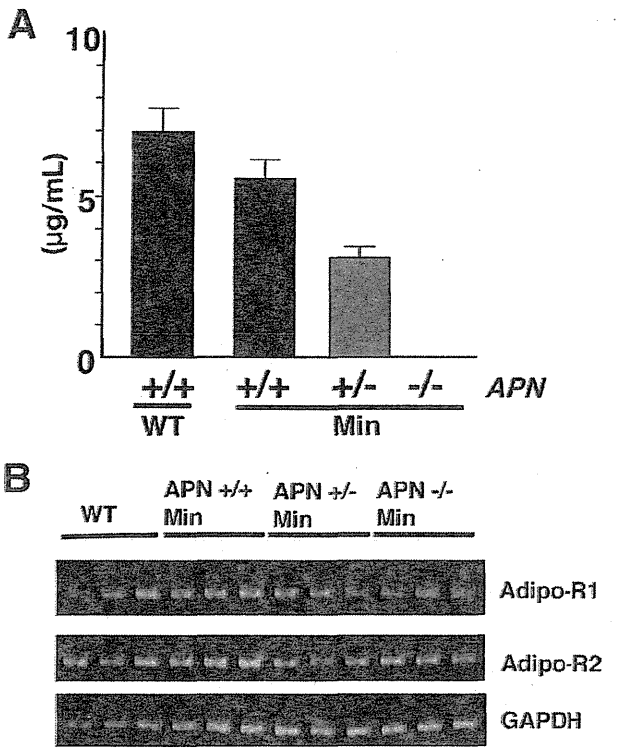

Figure 1. Serum adiponectin (APN) levels and expression levels of APN receptors in *APN*-deficient *Min* mice. (*A*) Serum APN levels for 12-week-old male $APN^{+/+}$*Min*, $APN^{+/-}$*Min*, and $APN^{-/-}$*Min* mice (n = 3) and for 12-week-old male $APN^{+/+}$ mice (n = 4) were evaluated by enzyme-linked immunosorbent assay. (*B*) Liver samples from 12-week-old male *APN*-deficient *Min* mice (n = 3) and for 12-week-old male $APN^{+/+}$ C57BL/6J mice (n = 3) were analyzed for APN receptors, Adipo-R1 and -R2 by reverse transcription polymerase chain reaction analysis. Glyceraldehyde-3-phosphate dehydrogenase was employed as an internal control. WT, wild-type mice.

Table 1. Number of Intestinal Polyps in Male Adiponectin-Deficient *Min* Mice

		No. of polyps/mouse				
		Small intestine				
Age (*wk*)	APN genotype	Proximal	Middle	Distal	Colon	Total
9	+/+	2.1 ± 0.6	8.4 ± 2.7	29.6 ± 11.5	0.1 ± 0.1	40.4 ± 14.5
	+/−	3.6 ± 0.8	23.6 ± 3.4[a]	68.6 ± 9.9[b]	0.7 ± 0.3	96.4 ± 12.3[b]
	−/−	4.0 ± 0.6[b]	26.4 ± 2.3[a]	97.9 ± 12.4[a]	1.1 ± 0.3[b]	128.0 ± 14.2[a]
12	+/+	4.4 ± 1.3	17.1 ± 3.9	52.9 ± 8.8	1.3 ± 0.5	75.7 ± 13.5
	+/−	5.7 ± 1.0	41.5 ± 5.5[a]	130.7 ± 6.6[a]	1.7 ± 0.6	179.2 ± 10.8[a]
	−/−	8.1 ± 1.4	34.7 ± 4.2[b]	111.7 ± 11.2[a]	2.0 ± 0.5	156.6 ± 15.3[a]

NOTE. Data are mean ± standard error (n = 7).
APN, adiponection.
[a]$P < .01$ vs *APN*$^{+/+}$*Min*.
[b]$P < .05$ vs *APN*$^{+/+}$*Min*.

APN$^{+/+}$*Min* mice, a tendency for increase was observed at 9 and 12 weeks of age. Serum levels of total cholesterol were not largely altered with the age and genotypes (Supplementary Figure 1). Similar results regarding serum TG and cholesterol were obtained in female *APN*-deficient *Min* mice.

Intestinal Polyp Formation by APN Knockout Mutation in Min *Mice*

Table 1 shows data for the number and distribution of intestinal polyps in the male *APN*$^{+/+}$*Min*, *APN*$^{+/-}$*Min* and *APN*$^{-/-}$*Min* mice at the 9 and 12 weeks, while data for female mice are given in Supplementary Table 1. The polyps developing in each genotype were all histopathologically identified as adenomas. Development of intestinal polyps in the male *APN*$^{+/-}$*Min* and *APN*$^{-/-}$*Min* mice at 9 weeks were 239% and 317% of the total value in male *APN*$^{+/+}$*Min* mice, respectively, and 319% and 338% of total value in female *APN*$^{+/+}$*Min* mice. At 12 weeks, male *APN*$^{+/-}$*Min* and *APN*$^{-/-}$*Min* mice developed polyps at 237% and 207% of the total value in male *APN*$^{+/+}$*Min* mice, respectively, and 230% and 206% of those in female mice. Representative photographs of the intestinal polyps observed in the male *APN*$^{+/+}$*Min*, *APN*$^{+/-}$*Min*, and *APN*$^{-/-}$*Min* mice at 12 weeks are shown in Supplementary Figure 2.

To confirm the effects of APN on intestinal polyp formation, APN was intraperitoneally injected to *APN*$^{+/-}$*Min* mice. The total number of intestinal polyps was significantly less in the APN-injected group than in saline-injected group in both sexes, as shown in Supplementary Table 2 and Supplementary Figure 2.

Change of Serum Levels of Adipocytokines in APN-Deficient Min *Mice*

In an attempt to clarify mechanisms affecting development of intestinal polyps, we analyzed serum levels for other adipocytokines, including Pai-1, leptin, resistin, TNFα, IL-6, and MCP-1. Among the adipocytokines, Pai-1 levels were significantly increased 1.5-fold and 2.1-fold ($P < .05$) in 12-week-old male *APN*$^{+/-}$*Min* and *APN*$^{-/-}$*Min* mice as compared with *APN*$^{+/+}$*Min* mice, respectively (Table 2), and were also increased in 9-week-old male *APN*$^{+/-}$*Min* and *APN*$^{-/-}$*Min* mice. Serum leptin levels were slightly decreased with APN deficiency. Resistin, TNFα, IL-6, and MCP-1 levels did not appear to depend on the genotypes.

Table 2. Serum Adipocytokine Concentrations in Male Adiponectin-Deficient *Min* Mice

Age (*wk*)	APN genotype	Pai-1, *pg/mL*	Leptin, *pg/mL*	Resistin, *pg/mL*	TNFα, *pg/mL*	IL-6, *pg/mL*	MCP-1, *pg/mL*
9	+/+	1319 ± 108	3632 ± 859	1450 ± 121	5.0 ± 0.4	15 ± 5	35 ± 5
	+/−	1819 ± 117[a]	3163 ± 544	1281 ± 92	5.0 ± 0.3	12 ± 6	32 ± 5
	−/−	1738 ± 105[a]	3196 ± 783	1299 ± 110	5.1 ± 0.3	32 ± 11	34 ± 5
12	+/+	5131 ± 2540	3210 ± 938	989 ± 72	4.7 ± 0.2	20 ± 7	22 ± 6
	+/−	7451 ± 1425	2014 ± 253	1189 ± 133	5.7 ± 0.5	27 ± 6	13 ± 1
	−/−	10693 ± 4542[b]	1792 ± 562	1152 ± 562	6.0 ± 0.6	23 ± 12	19 ± 1

NOTE. Data are mean ± standard error (n = 4–5).
APN, adiponectin; IL-6, interleukin-6; MCP-1, monocyte chemotactic protein-1; Pai-1, plasminogen activator inhibitor–1; TNFα, tumor necrosis factor–α.
[a]$P < .05$ vs 9-week-old *APN*$^{+/+}$*Min*.
[b]$P < .05$ vs 12-week-old *APN*$^{+/+}$*Min*.

Table 3. Incidence and Multiplicity of Azoxymethane-Induced Colon Tumor in Male Adiponectin-Deficient Mice

	Adenoma		Adenocarcinoma		Total	
APN genotype	Incidence (%)	Multiplicity[a]	Incidence (%)	Multiplicity[a]	Incidence (%)	Multiplicity[a]
+/+	4/25 (16)	0.2 ± 0.5	7/25 (28)	0.3 ± 0.6	10/25 (40)	0.5 ± 0.7
+/−	6/28 (21)	0.2 ± 0.4	9/28 (32)	0.4 ± 0.6	14/28 (50)	0.6 ± 0.7
−/−	8/24 (33)	0.3 ± 0.5	12/24 (50)	0.8 ± 1.0	17/24 (71)[b]	1.1 ± 1.0[b]

APN, adiponectin.
[a]Data are mean ± standard deviation.
[b]$P < .05$ vs $APN^{+/+}$.

Colon Tumor Development in APN-Deficient C57BL/6J Mice With AOM Treatment

Male $APN^{+/+}$, $APN^{+/-}$, and $APN^{-/-}$ C57BL/6J mice were treated with AOM. The change of each genotype did not affect food intake, clinical signs, or body weight changes during the experimental period. At the end of the experiment, whole body fat ratios for C57BL/6J mice in each genotype with AOM treatment were almost the same (Supplementary Figure 3), and all genotypes demonstrated similar levels of serum TG, total cholesterol, high-density lipoprotein, and free fatty acids (Supplementary Figure 3).

Data for the incidence and multiplicity of colon tumors are summarized in Table 3. No lesions were apparent without the carcinogen. Total tumor incidences were increased to 50% and 71% ($P < .05$) in $APN^{+/-}$ and $APN^{-/-}$ C57BL/6J mice, respectively, as compared with 40% in wild-type mice. Regarding tumor multiplicity, values were 0.5, 0.6, and 1.1 ($P < .05$) for $APN^{+/+}$, $APN^{+/-}$, and $APN^{-/-}$ C57BL/6J mice, respectively. Histopathological examination revealed that incidence of adenoma in wild-type mice was 16% and adenocarcinoma was 28%, and each incidence tended to be increased with APN deficiency. Moreover, multiplicity of adenocarcinoma tended to be increased with APN deficiency. Average colon tumor diameters for $APN^{+/+}$, $APN^{+/-}$, and $APN^{-/-}$ C57BL/6J mice were 2.8 ± 1.5 (mean ± standard deviation), 3.0 ± 0.9 and 3.4 ± 1.6 mm, respectively.

Change of Adipocytokine Levels by APN Gene Deficiency

We also analyzed serum levels for adipocytokines in 55-week-old male APN-deficient C57BL/6J mice treated with AOM. Among the adipocytokines, Pai-1 levels increased 1.6-fold and 1.7-fold in $APN^{+/-}$ and $APN^{-/-}$ C57BL/6J mice as compared to those in $APN^{+/+}$ C57BL/6J mice, respectively (Table 4). Pai-1 is expressed ubiquitously. Thus, representative Pai-1 expression levels were analyzed using liver samples. Hepatic Pai-1 mRNA levels for 55-week-old male $APN^{+/-}$ and $APN^{-/-}$ C57BL/6J mice increased 1.8-fold and 1.4-fold compared to those in $APN^{+/+}$ mice, respectively. Serum TNFα and MCP-1 levels were slightly decreased in $APN^{+/-}$ and $APN^{-/-}$ C57BL/6J mice compared to those in wild-type mice. Leptin, resistin, and IL-6 levels did not depend on the genotypes.

Analysis of AMPK Activity

To investigate whether AMPK is involved in the regulation of Pai-1, *Min* mice were fed an AMPK activator, metformin, for 14 weeks. Hepatic mRNA levels for Pai-1 in metformin-treated *Min* mice decreased to 28% ($P < .05$) of those in untreated *Min* mice.

To confirm the known molecular signaling from Adipo-R1 that affects the development of intestinal tumors, we analyzed p-AMPK levels in small intestinal epithelial cells. In 9-week-old male $APN^{+/-}$ and $APN^{-/-}$ C57BL/6J mice they were reduced to 53% and 37% of those in $APN^{+/+}$ C57BL/6J mice, respectively (Figure 2*A*). P-AMPK levels in colon epithelial cells also tended to be reduced with APN deficiency (Figure 2*B*). P-AMPK levels in the liver were slightly reduced in APN-deficient *Min* mice (Figure 2*C*). Furthermore, p-Akt levels in intestinal epithelial cells were elevated in $APN^{-/-}$ C57BL/6J mice (Figure 2*D*).

To confirm the existence of AdipoR-binding proteins, RACK1 and CK2β, which regulate proximal signal transduction events in response to APN, immuno-

Table 4. Serum Adipocytokine Concentrations in Azoxymethane-Treated Male Adiponectin-Deficient Mice

APN genotype	Pai-1, *pg/mL*	Leptin, *pg/mL*	Resistin, *pg/mL*	TNFα, *pg/mL*	IL-6, *pg/mL*	MCP-1, *pg/mL*
+/+	1998 ± 249	4612 ± 576	4015 ± 322	44 ± 10	65 ± 12	114 ± 16
+/−	3220 ± 293[a]	3693 ± 558	3554 ± 366	36 ± 4	71 ± 23	103 ± 15
−/−	3470 ± 776	4326 ± 850	4742 ± 274	36 ± 5	69 ± 12	85 ± 12

NOTE. Data are mean ± standard error (n = 10).
APN, adiponectin; IL-6, interleukin-6; MCP-1, monocyte chemotactic protein-1; Pai-1, plasminogen activator inhibitor−1; TNFα, tumor necrosis factor−α.
[a]$P < .01$ vs $APN^{+/+}$.

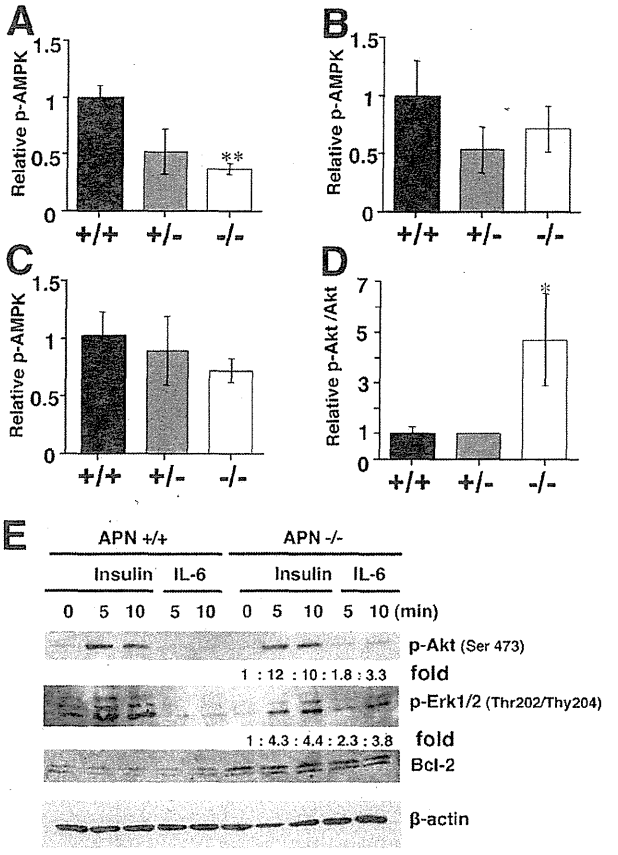

Figure 2. Phosphorylated–AMP-activated protein kinase (p-AMPK) and -Akt levels in adiponectin (*APN*)-deficient mice and its derived fibroblasts. Relative p-AMPK levels in the small intestine (*A*) and colon (*B*) of 9-week-old male $APN^{+/+}$, $APN^{+/-}$, and $APN^{-/-}$ C57BL/6J mice without azoxymethane treatment (n = 4 each), respectively, were evaluated by enzyme-linked immunosorbent assay (ELISA). (*C*) Relative p-AMPK levels in the liver of 12-week-old male $APN^{+/+}$*Min*, $APN^{+/-}$*Min*, and $APN^{-/-}$*Min* mice (n = 4 each) were evaluated by ELISA. (*D*) Relative p-Akt/total Akt levels in the small intestine of AOM-treated 55-week-old male $APN^{+/+}$, $APN^{+/-}$, and $APN^{-/-}$ C57BL/6J mice (n = 6 each) were evaluated by ELISA. *Black*, $APN^{+/+}$; *gray*, $APN^{+/-}$; *white*, $APN^{-/-}$. Data are mean ± standard error. $^{**}P < .01$. $^{*}P < .05$. (*E*) Effects of insulin (1 μg/mL for 5 and 10 minutes treatment) and interleukin-6 (IL-6; 50 ng/mL for 5 and 10 minutes) on the protein expression of p-Akt and -Erk, and Bcl-2 in fibroblasts derived from $APN^{+/+}$ and $APN^{-/-}$ C57BL/6J mice are shown. β-actin was a loading control. Density of the bands was evaluated by NIH image, and the relative level was further normalized by β-actin.

histochemical analysis was performed on the colon tumors of 55-week-old male $APN^{+/+}$, $APN^{+/-}$, and $APN^{-/-}$ C57BL/6J mice treated with AOM and small intestinal polyps of 9-week-old male $APN^{+/+}$*Min*, $APN^{+/-}$*Min*, and $APN^{-/-}$*Min* mice. RACK1 and CK2β were expressed in the epithelial cells of normal colon mucosa and colon tumor at the almost same levels in each genotype (Supplementary Figures 4 and 5). Real-time PCR revealed that the expression levels of CK2β were almost the same among the colon mucosa of 9-week-old male $APN^{+/+}$, $APN^{+/-}$, and $APN^{-/-}$ C57BL/6J mice (data not shown). The expression levels of RACK1 and CK2β were weakly observed in the nontumorous parts and intestinal polyps of *Min* mice, and expressions were at almost the same levels in each genotype (Supplementary Figures 4 and 5).

Effects of Pai-1 Blocker on Colon ACF Development in $APN^{-/-}$ C57BL/6J Mice With AOM Treatment

To clarify if Pai-1 might be involved in colon carcinogenesis, we used a short-term in vivo model using ACF formation induced by AOM. The mean body weights of the AOM-treated $APN^{-/-}$ C57BL/6J mice were not affected by administration of 50, 100 ppm SK-216, Pai-1 blocker. In APN-deficient C57BL/6J mice with 0, 50, 100 ppm SK-216 treatment, the mean numbers of ACFs/colon were 27.7, 23.1, and 18.4 ($P < .05$), respectively (Supplementary Table 3). Thus, Pai-1 blocker decreased colon ACF development in $APN^{-/-}$ C57BL/6J mice with AOM treatment.

Effects of APN Deficiency on Signal Transduction Events in Primary Cultured Cells

To study what happens to cell function in the absence of APN, fibroblasts were prepared from newborn $APN^{+/+}$ and $APN^{-/-}$ C57BL/6J mouse epidermis and treated with cell growth stimuli, insulin, or IL-6. Insulin treatment increased p-Akt and -Erk1/2 levels in both fibroblasts (Figure 2*E*). Interestingly, p-Akt and -Erk1/2 levels were increased 3.3- and 3.8-fold, respectively, by the treatment with IL-6 for 10 minutes in APN-knockout fibroblasts. Moreover, Bcl-2 was clearly expressed in APN-knockout fibroblasts compared with APN-wild fibroblasts.

Discussion

This study provided evidence that APN plays a pivotal role in intestinal carcinogenesis in mice. Thus, APN-deficient *Min* mice showed a 2- or 3-fold increase in the total number of intestinal polyps compared to those of APN-wild *Min* mice in both males and females at the ages of 9 and 12 weeks. In addition, APN-deficient *Min* mice exhibited increased serum Pai-1 levels with the *APN*-gene dosage. In addition, APN-deficient C57BL/6J mice treated with AOM demonstrated increased incidences and multiplicities of colorectal tumors, again with gene dosage-dependence, and serum Pai-1 levels tended to be increased with APN-deficiency at the age of 55 weeks.

In the $APN^{+/-}$ *Min* mice, serum APN levels were almost half those of $APN^{+/+}$*Min* mice, consistent with the gene dosage. Serum APN was not detected in $APN^{-/-}$*Min* mice. Numbers of intestinal polyps in *Min* mice were also associated with *APN*-gene dosage (Table 1 and Supplementary Table 1). Moreover, the effects of APN deficiency could be reversed by administration of APN (Supplemen-

tary Table 2). Other factors that might affect intestinal polyp development were not largely changed. For instance, expression levels of APN receptors, Adipo-R1 and -R2, and AdipoR-binding proteins, RACK1 and CK2β, were not affected by the genotype. Body weights and serum lipid levels also did not significantly vary. Of note, serum TG levels increased age dependently and also with a tendency for increase with the *APN*-gene dosage (Supplementary Figure 1). These data indicated that the amount of APN strongly affects development of intestinal polyps. In 12-week-old *APN*$^{-/-}$*Min* mice, the number of intestinal polyps was slightly decreased compared to those of *APN*$^{+/-}$*Min* mice. Several factors, such as an achievement of maximum levels of polyp development, serum TG levels, or some general dysfunctions, may influence polyp numbers, but further examinations are needed to clarify mechanisms.

It has been reported that 22-week short-term administration of a high-fat diet, but not normal diet, enhanced ACFs and tumor development in the colon of APN-deficient C57BL/6J mice.[21] The discrepancy in results between our study and this previous report could be due to the differences in the experimental period and diet. We followed the previous chemical-induced carcinogenesis protocol[22,23] and our findings added evidence that APN itself can suppress development of colon cancer under normal diet condition. It is assumed that abolished signaling from Adipo-R1 could enhance cell growth. It is known that activation of AMPK is decreased with APN deficiency in the colon epithelial cells. AMPKα activation through Adipo-R1 inhibits Akt followed by mammalian target of rapamycin inactivation.[21,24] The phosphatidylinositol 3 kinase/Akt signal pathway has been reported to activate signals for cell survival, cell growth, and the cell cycle leading to carcinogenesis.[25] We confirmed that abolished signaling from Adipo-R1 reduces AMPK activation (Figure 2*A*, *B*, and *C*), and increases Akt activation (Figure 2*D*). Therefore, we suggest that the AMPK/mammalian target of rapamycin/Akt pathway is possibly involved in the protective effect of APN against colon carcinogenesis. Moreover, primary cell cultures of fibroblasts from *APN*$^{+/+}$ or *APN*$^{-/-}$ C57BL/6J mice indicated that cells lacking APN are relatively responsive to growth stimuli and resistant to apoptosis through expressing Bcl-2,[26] which may support the growth advantage of neoplastic cells in APN-deficient mice.

APN acts as a regulator of adipocytokines. Under starvation conditions, APN activates AMPK in the hypothalamus to promote food intake and inhibits leptin activation.[27] In peripheral tissues, such as skeletal muscle, APN activates AMPK, IRS-1, and FATP-1, to stimulate fatty-acid combustion and glucose intake, which are inhibited by TNFα activation. It is assumed that APN deficiency affects other adipocytokine production in vivo, and can also affect intestinal tumorigenesis. Indeed, in the present study, serum levels of Pai-1 were significantly increased in the *APN*$^{+/-}$ and *APN*$^{-/-}$ C57BL/6J and *Min* mice. Treatment with an AMPK activator also reduced hepatic Pai-1 mRNA levels in *Min* mice, in line with earlier reports.[28,29] Thus, it is conceivable that Pai-1 expression levels are usually depressed by APN through Adipo-R1 receptor activity. We have recently demonstrated that Pai-1 blockers suppress intestinal polyp development in *Min* mice.[11] Thus, increased expression of Pai-1 could affect intestinal polyp development in *APN*$^{+/-}$*Min* and *APN*$^{-/-}$*Min* mice. Moreover, Pai-1 blocker was shown to decrease AOM-induced colon ACF formation in *APN*$^{-/-}$ C57BL/6J mice, indicating that increased expression of Pai-1 could affect colon carcinogenesis in *APN*$^{+/-}$ and *APN*$^{-/-}$ C57BL/6J mice.

In conclusion, this study indicated that hypoadiponectinemia promotes intestinal polyp development in *Min* mice, and also colon tumor development in AOM-treated C57BL/6J mice. AMPK inactivation belonging with Pai-1 induction and Akt activation was suggested to be the underlying mechanism for lack of APN on tumor growth. Further development of reagents that could elevate concentrations of APN is of interest. APN receptor agonists could be candidates for chemopreventive agents against colorectal cancer. Furthermore, as it is becoming more evident that a metabolic syndrome status promotes carcinogenesis in rodents and human, our results provide clues to a better understanding of mechanisms underlying colorectal carcinogenesis.

Supplementary Material

Note: To access the supplementary material accompanying this article, visit the online version of *Gastroenterology* at www.gastrojournal.org, and at doi: 10.1053/j.gastro.2011.02.019.

References

1. Trevisan M, Liu J, Muti P, et al. Markers of insulin resistance and colorectal cancer mortality. Cancer Epidemiol Biomarkers Prev 2001;10:937–941.
2. Colangelo LA, Gapstur SM, Gann PH, et al. Colorectal cancer mortality and factors related to the insulin resistance syndrome. Cancer Epidemiol Biomarkers Prev 2002;11:385–391.
3. Ahmed RL, Schmitz KH, Anderson KE, et al. The metabolic syndrome and risk of incident colorectal cancer. Cancer 2006;107: 28–36.
4. Stocks T, Lukanova A, Johansson M, et al. Components of the metabolic syndrome and colorectal cancer risk; a prospective study. Int J Obes (Lond) 2008;32:304–314.
5. Giovannucci E. Insulin and colon cancer. Cancer Causes Control 1995;6:164–179.
6. Matsuzawa Y. The metabolic syndrome and adipocytokines. FEBS Lett 2006;580:2917–2921.
7. Otake S, Takeda H, Suzuki Y, et al. Association of visceral fat accumulation and plasma adiponectin with colorectal adenoma: evidence for participation of insulin resistance. Clin Cancer Res 2005;11:3642–3646.
8. Yamauchi T, Kamon J, Ito T, et al. Cloning of adiponectin receptors that mediate antidiabetic metabolic effects. Nature 2003; 423:762–769.

9. Niho N, Takahashi M, Shoji Y, et al. Dose-dependent suppression of hyperlipidemia and intestinal polyp formation in Min mice by pioglitazone, a PPAR gamma ligand. Cancer Sci 2003;94:960–964.
10. Niho N, Takahashi M, Kitamura T, et al. Concomitant suppression of hyperlipidemia and intestinal polyp formation in APC-deficient mice by peroxisome proliferators-activated receptor ligands. Cancer Res 2003;63:6090–6095.
11. Mutoh M, Niho N, Komiya M, et al. Plasminogen activator inhibitor-1 (Pai-1) blockers suppress intestinal polyp formation in Min mice. Carcinogenesis 2008;29:824–829.
12. Kubota N, Terauchi Y, Yamauchi T, et al. Disruption of adiponectin causes insulin resistance and neointimal formation. J Biol Chem 2002;277:25863–25866.
13. Berg AH, Combs TP, Du X, Brownlee M, Scherer PE. The adipocyte-secreted protein Acrp30 enhances hepatic insulin action. Nat Med 2001;7:947–953.
14. Yamauchi T, Kamon J, Waki H, et al. The fat-derived hormone adiponectin reverses insulin resistance associated with both lipoatrophy and obesity. Nat Med 2001;7:941–946.
15. Otani K, Kitayama J, Yasuda K, et al. Adiponectin suppresses tumorigenesis in $Apc^{Min/+}$ mice. Cancer Lett 2010;288:177–182.
16. Sutherland LA, Bird RP. The effect of chenodeoxycholic acid on the development of aberrant crypt foci in the rat colon. Cancer Lett 1994;76:101–107.
17. Tsuchida A, Yamauchi T, Ito Y, et al. Insulin/Foxo1 pathway regulates expression levels of adiponectin receptors and adiponectin sensitivity. J Biol Chem 2004;279:30817–30822.
18. Ploplis VA, Balsara R, Sandoval-Cooper MJ, et al. Enhanced in vitro proliferation of aortic endothelial cells from plasminogen activator inhibitor-1-deficient mice. J Biol Chem 2004;279:6143–6151.
19. Li X, Shi X, Liang DY, Clark JD. Spinal CK2 regulates nociceptive signaling in models of inflammatory pain. Pain 2005;115:182–190.
20. Yuspa SH, Harris CC. Altered differentiation of mouse epidermal cells treated with retinyl acetate *in vitro*. Exp Cell Res 1974;86:95–105.
21. Fujisawa T, Endo H, Tomimoto A, et al. Adiponectin suppresses colorectal carcinogenesis under the high-fat diet condition. Gut 2008;57:1531–1538.
22. Shoji Y, Takahashi M, Kitamura T, et al. Downregulation of prostaglandin E receptor subtype EP3 during colon cancer development. Gut 2004;53:1151–1158.
23. Kawamori T, Kitamura T, Watanabe K, et al. Prostaglandin E receptor subtype EP1 deficiency inhibits colon cancer development. Carcinogenesis 2005;26:353–357.
24. Luo Z, Saha AK, Xiang X, et al. AMPK, the metabolic syndrome and cancer. Trends Pharmacol Sci 2005;26:69–76.
25. Huang XF, Chen JZ. Obesity, the PI3K/Akt signal pathway and colon cancer. Obes Rev 2009;10:610–616.
26. Konturek PC, Burnat G, Rau AT, Hahn EG, Konturek S. Effect of adiponectin and ghrelin on apoptosis of Barrett adenocarcinoma cell line. Dig Dis Sci 2008;53:597–605.
27. Kubota N, Yano W, Kubota T, et al. Adiponectin stimulates AMP-activated protein kinase in the hypothalamus and increases food intake. Cell Metab 2007;6:55–68.
28. Anfosso F, Chomiki N, Alessi MC, et al. Plasminogen activator inhibitor-1 synthesis in human hepatoma cell line Hep G2. Metformin inhibits the stimulating effect of insulin. J Clin Invest 1993;91:2185–2193.
29. He G, Pedersen SB, Bruun JM, et al. Metformin, but not thiazolidinediones, inhibits plasminogen activator inhibitor-1 production in human adipose tissue in vitro. Horm Metab Res 2003;35:18–23.

Received January 14, 2010. Accepted February 14, 2011.

Reprint requests

Address requests for reprints to: Michihiro Mutoh, MD, PhD, Cancer Prevention Basic Research Project, National Cancer Center Research Institute, 5-1-1 Tsukiji, Chuo-ku, Tokyo 104-0045, Japan. e-mail: mimutoh@ncc.go.jp; fax: +81-3-3543-9305.

Conflicts of interest

The authors disclose no conflicts.

Funding

This work was supported by Grants-in-Aid for Cancer Research, for the Third-Term Comprehensive 10-Year Strategy for Cancer Control from the Ministry of Health, Labour, and Welfare of Japan, and by the grant provided by The Ichiro Kanehara Foundation.

Supplementary Table 1. Number of Intestinal Polyps in Female Adiponectin-Deficient *Min* Mice

		No. of polyps/mouse				
		Small intestine				
Ages (wk)	APN genotype	Proximal	Middle	Distal	Colon	Total
9	+/+	2.6 ± 1.2	12.8 ± 4.7	36.4 ± 14.6	0.2 ± 0.2	52.0 ± 20.5
	+/−	4.0 ± 0.8	32.5 ± 7.0	128.7 ± 18.1[a]	0.5 ± 0.2	165.7 ± 25.6[a]
	−/−	5.6 ± 0.6[b]	37.1 ± 2.6[a]	132.3 ± 4.8[a]	1.0 ± 0.3	176.0 ± 5.6[a]
12	+/+	4.3 ± 1.2	19.4 ± 4.3	53.0 ± 12.8	0.1 ± 0.1	76.9 ± 17.7
	+/−	6.9 ± 1.6	46.0 ± 8.5[b]	123.0 ± 13.0[a]	1.0 ± 0.4	176.9 ± 22.0[a]
	−/−	6.4 ± 1.1	35.3 ± 1.6[a]	115.0 ± 9.8[a]	1.4 ± 0.4	158.1 ± 9.7[a]

NOTE. Data are mean ± standard error.
APN, adiponectin.
[a]$P < .01$ vs *APN*$^{+/+}$*Min*.
[b]$P < .05$ vs *APN*$^{+/+}$*Min*.

Supplementary Table 2. Number of Intestinal Polyps in 12-Week-Old *APN*$^{+/-}$*Min* Mice Treated With or Without Adiponectin

		No. of polyps/mouse				
		Small intestine				
Sex	APN (IP)	Proximal	Middle	Distal	Colon	Total
Male	–	5.4 ± 0.9	35.0 ± 4.9	103.6 ± 14.1	1.2 ± 0.4	145.2 ± 18.4
		3.3 ± 0.6	9.3 ± 1.5[a]	26.1 ± 6.2[a]	0.8 ± 0.3	39.5 ± 7.9[a]
Female	–	4.0 ± 0.8	25.2 ± 3.2	70.7 ± 11.5	0.6 ± 0.3	100.5 ± 14.9
		3.4 ± 0.9	12.5 ± 3.1[b]	27.9 ± 8.2[a]	0.2 ± 0.1	44.0 ± 12.0[a]

NOTE. Data are mean ± standard error (n = 10).
APN, adiponectin; IP, intraperitoneal.
[a]$P < .01$ vs corresponding sex without APN treatment.
[b]$P < .05$ vs corresponding sex without APN treatment.

Supplementary Table 3. Number of Azoxymethane-Induced Colonic Aberrant Crypt Foci in *APN*−/−C57BL/6J Mice Treated With SK-216

		No. of aberrant crypt foci/colon				
SK-216 (ppm)	No. of animals	Proximal	Middle	Distal	Rectum	Total
0	8	0.4 ± 0.2	3.6 ± 1.0	12.6 ± 1.6	11.0 ± 2.3	27.7 ± 3.4
50	9	0.7 ± 0.3	1.9 ± 0.6	12.7 ± 1.5	7.9 ± 0.7	23.1 ± 2.1
100	8	0.0	1.6 ± 0.7	9.6 ± 1.0	7.1 ± 1.7	18.4 ± 1.9[a]

NOTE. Data are mean ± standard error.
[a]$P < .05$ vs 0 ppm.

Blockade of class IB phosphoinositide-3 kinase ameliorates obesity-induced inflammation and insulin resistance

Naoki Kobayashi[a], Kohjiro Ueki[a,b,1], Yukiko Okazaki[a], Aya Iwane[a], Naoto Kubota[a,b,c], Mitsuru Ohsugi[a], Motoharu Awazawa[a,c], Masatoshi Kobayashi[a], Takayoshi Sasako[a], Kazuma Kaneko[a], Miho Suzuki[a], Yoshitaka Nishikawa[a], Kazuo Hara[a], Kotaro Yoshimura[d], Isao Koshima[d], Susumu Goyama[e], Koji Murakami[f], Junko Sasaki[g], Ryozo Nagai[h], Mineo Kurokawa[e], Takehiko Sasaki[g], and Takashi Kadowaki[a,b,c,1]

[a]Department of Metabolic Diseases, [d]Department of Plastic Surgery, [e]Department of Hematology and Oncology, and [h]Department of Cardiovascular Medicine, Graduate School of Medicine, and [b]Translational Systems Biology and Medicine Initiative (TSBMI), University of Tokyo, Tokyo 113-0033, Japan; [c]Division of Applied Nutrition, National Institute of Health and Nutrition, Tokyo 162-8636, Japan; [f]Discovery Research Laboratories, Kyorin Pharmaceutical Co., Ltd., Tochigi 329-0114, Japan; and [g]Division of Microbiology, Department of Pathology and Immunology, Akita University School of Medicine, Akita 010-8543, Japan

Edited* by Lewis Clayton Cantley, Beth Israel Deaconess Medical Center, Boston, MA, and approved February 23, 2011 (received for review November 2, 2010)

Obesity and insulin resistance, the key features of metabolic syndrome, are closely associated with a state of chronic, low-grade inflammation characterized by abnormal macrophage infiltration into adipose tissues. Although it has been reported that chemokines promote leukocyte migration by activating class IB phosphoinositide-3 kinase (PI3Kγ) in inflammatory states, little is known about the role of PI3Kγ in obesity-induced macrophage infiltration into tissues, systemic inflammation, and the development of insulin resistance. In the present study, we used murine models of both diet-induced and genetically induced obesity to examine the role of PI3Kγ in the accumulation of tissue macrophages and the development of obesity-induced insulin resistance. Mice lacking p110γ (*Pik3cg*$^{-/-}$), the catalytic subunit of PI3Kγ, exhibited improved systemic insulin sensitivity with enhanced insulin signaling in the tissues of obese animals. In adipose tissues and livers of obese *Pik3cg*$^{-/-}$ mice, the numbers of infiltrated proinflammatory macrophages were markedly reduced, leading to suppression of inflammatory reactions in these tissues. Furthermore, bone marrow-specific deletion and pharmacological blockade of PI3Kγ also ameliorated obesity-induced macrophage infiltration and insulin resistance. These data suggest that PI3Kγ plays a crucial role in the development of both obesity-induced inflammation and systemic insulin resistance and that PI3Kγ can be a therapeutic target for type 2 diabetes.

Type 2 diabetes and metabolic syndrome, the major risk factors of cardiovascular disease and related death, are explosively increasing worldwide due to a pandemic of obesity that induces a variety of disorders, such as insulin resistance and hepatic steatosis (1, 2). Recent studies have revealed that obesity induces hematopoietic cell infiltration into adipose tissue, which in turn enhances adipose tissue inflammation and the secretion of proinflammatory adipokines, leading to systemic insulin resistance (3–8). Inhibition of macrophage infiltration into adipose tissue could be considered a therapeutic strategy on the basis of the accumulated evidence of obesity-related metabolic disorders.

It has been known that chemokines initiate chemotaxis by binding the corresponding G protein-coupled receptors (GPCRs), leading to activation of class IB phosphoinositide-3 kinase (PI3Kγ) (9). Upon chemokine stimulation, the unidirectional cytoskeletal rearrangement caused by PI3Kγ promotes cell movement toward the higher concentration of the chemokine. Furthermore, previous studies using mice lacking p110γ (*Pik3cg*$^{-/-}$ mice), the catalytic subunit of the PI3Kγ complex, demonstrated that PI3Kγ is essential for chemotaxis in leukocytes, including macrophages (10, 11). However, the role of PI3Kγ in obesity-induced macrophage infiltration into tissues, systemic inflammation, and the development of insulin resistance is still unknown.

To investigate the role of PI3Kγ in obesity-induced insulin resistance, we analyzed *Pik3cg*$^{-/-}$ mice fed a high-fat diet (HFD) and those with a genetically obese diabetic background and found that these mice exhibit improved insulin sensitivity along with decreased macrophage infiltration and inflammatory changes. Moreover, we have also demonstrated that a pharmacological inhibitor of PI3Kγ ameliorates obesity-induced diabetes.

Results

Mice Lacking PI3Kγ Were Protected from HFD-Induced Insulin Resistance. We fed *Pik3cg*$^{-/-}$ and wild-type control (*Pik3cg*$^{+/+}$) mice a normal diet (ND) or a HFD. While receiving ND, *Pik3cg*$^{-/-}$ mice grew normally and showed no significant differences in glucose metabolism, insulin sensitivity, and glucose tolerance compared with *Pik3cg*$^{+/+}$ mice (Fig. S1). These data suggest that PI3Kγ is not required for normal growth nor for maintenance of glucose homeostasis during ND conditions. In contrast, HFD-fed *Pik3cg*$^{-/-}$ mice maintained significantly lower blood glucose and insulin levels under random-fed conditions and also showed better response to insulin as estimated by an insulin tolerance test (ITT) (Fig. 1 *A–C*), indicating that lack of PI3Kγ led to protection from HFD-induced insulin resistance. Reflecting the improved systemic insulin sensitivity, insulin concentrations of *Pik3cg*$^{-/-}$ mice were significantly lower than those of *Pik3cg*$^{+/+}$ mice during the glucose tolerance test (GTT) whereas both groups of mice showed similar blood glucose levels (Fig. 1*D*). Furthermore, we observed significantly enhanced insulin signaling in liver and muscle of HFD-fed *Pik3cg*$^{-/-}$ mice (Fig. 1 *E* and *F* and Fig. S2). To investigate the impact of the lower weight gain of *Pik3cg*$^{-/-}$ mice compared with *Pik3cg*$^{+/+}$ mice under HFD-fed conditions without any differences in food intake and energy expenditure (Table S1), we fed *Pik3cg*$^{+/+}$ mice a limited HFD to match the weight gain of *Pik3cg*$^{-/-}$ mice. *Pik3cg*$^{-/-}$ mice still displayed better insulin sensitivity even compared with the weight-matched *Pik3cg*$^{+/+}$ mice (Fig. S3). These results suggest that PI3Kγ is required for HFD-induced systemic insulin resistance and that the body weight change does not seem to be a major cause of improved insulin sensitivity observed in HFD-fed *Pik3cg*$^{-/-}$ mice.

Author contributions: N. Kobayashi, K.U., and T.K. designed research; N. Kobayashi, K.U., Y.O., A.I., N. Kubota, M.O., M.A., M. Kobayashi, T. Sasako, K.K., M.S., Y.N., and S.G. performed research; K.Y., I.K., K.M., J.S., and T. Sasaki contributed new reagents/analytic tools; N. Kobayashi, K.U., K.H., R.N., and M. Kurokawa analyzed data; and N. Kobayashi, K.U., and T.K. wrote the paper.

The authors declare no conflict of interest.

*This Direct Submission article had a prearranged editor.

[1]To whom correspondence may be addressed. E-mail: ueki-tky@umin.ac.jp or kadowaki-3im@h.u-tokyo.ac.jp.

This article contains supporting information online at www.pnas.org/lookup/suppl/doi:10.1073/pnas.1016430108/-/DCSupplemental.

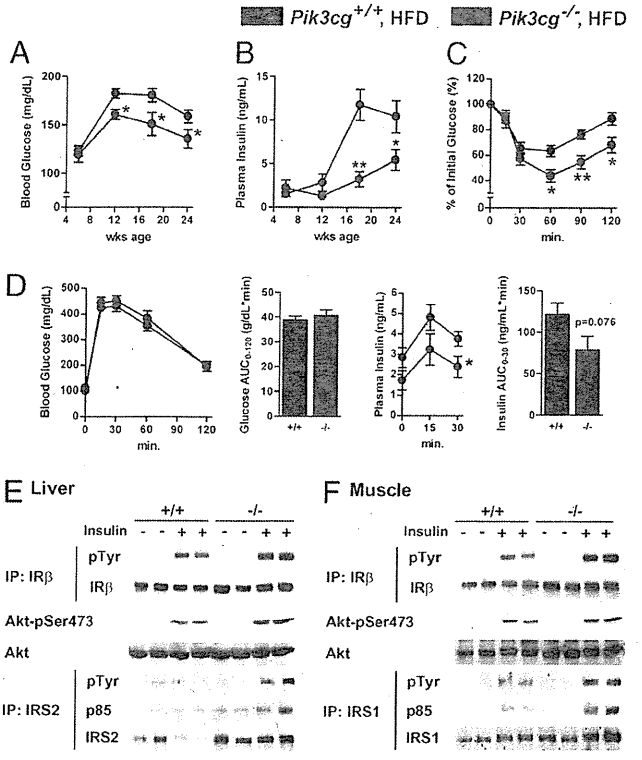

Fig. 1. Mice lacking PI3Kγ were protected from HFD-induced insulin resistance. (*A* and *B*) Blood glucose (*A*) and plasma insulin levels (*B*) in *Pik3cg*$^{+/+}$ and *Pik3cg*$^{-/-}$ mice fed on a HFD from 6 to 24 wk of age (n = 15–20). (*C*) Glucose levels during ITT (23 wk of age) were determined at the indicated time points after i.p. injection with a bolus of insulin [1.0 U·kg^{-1} body weight (BW)] (n = 7–8). (*D*) Glucose and insulin levels during GTT (24 wk of age) were determined at the indicated time points after i.p. injection with a bolus of glucose (1.5 g·kg^{-1} BW) (n = 7–8). (*E* and *F*) Phosphorylation of insulin receptor β-subunit (IRβ), insulin receptor substrate (IRS-1, IRS-2), and Akt induced by a bolus injection of insulin was assessed in livers (*E*) and skeletal muscles (*F*) of *Pik3cg*$^{+/+}$ ($^{+/+}$) and *Pik3cg*$^{-/-}$ ($^{-/-}$) mice fed a HFD (n = 3–4). IP, immunoprecipitated; pTyr, phosphorylated tyrosine; pSer, phosphorylated serine. $*P < 0.05$, $**P < 0.01$.

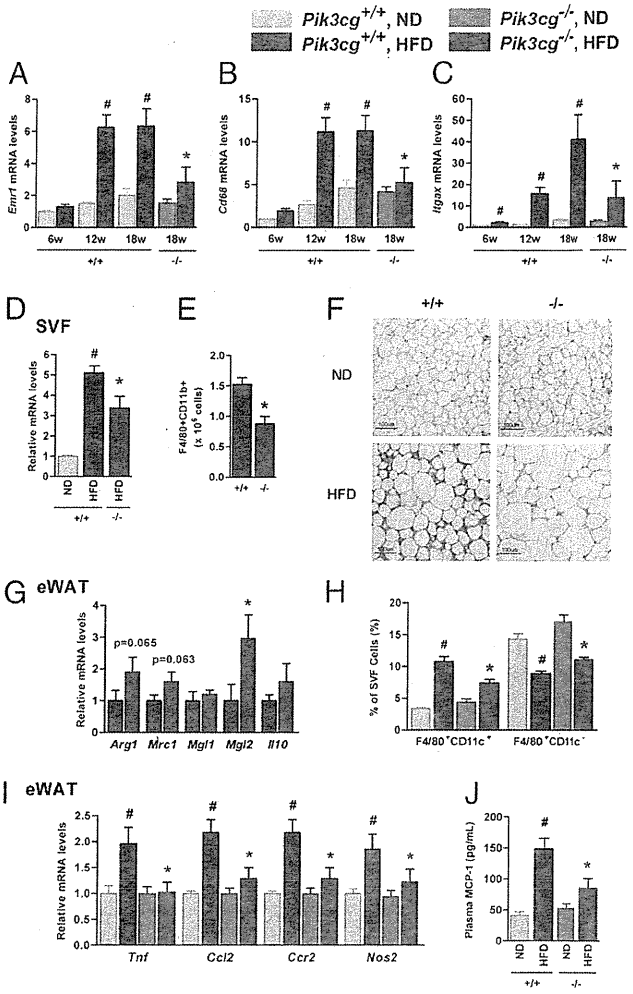

Fig. 2. Loss of PI3Kγ decreased macrophage infiltration into adipose tissue and markedly suppressed proinflammatory changes induced by a HFD. (*A–C*) Expression levels of *Emr1* (F4/80, *A*), *Cd68* (*B*), and *Itgax* (CD11c, *C*) in eWAT of *Pik3cg*$^{+/+}$ ($^{+/+}$) and *Pik3cg*$^{-/-}$ ($^{-/-}$) mice fed a ND or a HFD for the indicated periods (n = 6–8). (*D* and *E*) Expression levels of *Cd68* (*D*) and the population of macrophages (F4/80$^+$CD11b$^+$) measured by FACS analysis (*E*) in SVF from the eWAT (n = 4–5). (*F*) Immunohistochemical analysis of adipose tissue macrophages. eWAT of mice fed ND or HFD were stained with antibody against F4/80. (Scale bar, 100 μm.) (*G*) Expression levels of M2 macrophage-specific genes in eWAT of *Pik3cg*$^{+/+}$ and *Pik3cg*$^{-/-}$ mice fed on a HFD (normalized to *Cd68*) (n = 6–8). (*H*) Quantification of M1 macrophage (F4/80$^+$CD11c$^+$) and M2 macrophage (F4/80$^+$CD11c$^-$) in SVF from eWAT of mice fed on a ND or a HFD (n = 5). (*I*) Expression levels of proinflammatory genes in eWAT (n = 6–8). (*J*) Serum levels of MCP-1 in *Pik3cg*$^{+/+}$ and *Pik3cg*$^{-/-}$ mice fed on a ND or a HFD (n = 6–8). $\#P < 0.05$ for HFD compared with ND. $*P < 0.05$ for *Pik3cg*$^{-/-}$ mice compared with *Pik3cg*$^{+/+}$ controls.

Loss of PI3Kγ Markedly Decreased the Number of Infiltrated Macrophages and the Amount of Inflammation in Adipose Tissue Induced by HFD. To clarify the mechanisms leading to the improvement of HFD-induced insulin resistance, we investigated the infiltrated macrophage contents in the epididymal adipose tissue (eWAT) of *Pik3cg*$^{-/-}$ and *Pik3cg*$^{+/+}$ mice. HFD feeding progressively increased the expression of macrophage-specific markers in the eWAT of *Pik3cg*$^{+/+}$ mice (Fig. 2 *A* and *B*). By contrast, the levels of macrophage-specific markers were markedly decreased in the eWAT, particularly in the stromal vascular fraction of *Pik3cg*$^{-/-}$ mice under HFD-fed conditions (Fig. 2 *A*, *B*, and *D*), although no significant differences in adiposity, adipocyte size, and the expression levels of genes involved in adipocyte function were observed between *Pik3cg*$^{+/+}$ and *Pik3cg*$^{-/-}$mice (Fig. S4*A* and Table S1). Fluorescence-activated cell sorting (FACS) and histological analyses also showed significant reductions of adipose tissue macrophages (ATMs) in HFD-fed *Pik3cg*$^{-/-}$ mice (Fig. 2 *E* and *F*). Expression of *Itgax* (coding CD11c), which has been reported to increase in the eWAT of mice fed a HFD (12, 13), was markedly suppressed in *Pik3cg*$^{-/-}$ mice (Fig. 2*C*). By contrast, the relative levels of genes preferentially expressed in M2 macrophages (14) were increased in the eWAT of *Pik3cg*$^{-/-}$ mice (Fig. 2*G*). FACS analysis also revealed that HFD feeding in *Pik3cg*$^{+/+}$ mice decreased the F4/80$^+$CD11c$^-$ population in the stromal vascular cells of eWAT accompanied by a 3.2-fold increase in the F4/80$^+$CD11c$^+$ population (Fig. 2*H*). Conversely, *Pik3cg* deletion significantly decreased the HFD-induced F4/80$^+$CD11c$^+$ double-positive cells enrichment but not that of F4/80$^+$CD11c$^-$ in the eWAT of HFD-fed mice (Fig. 2*H*). These changes resulted in a shift-up in the ratio of M2 to M1 macrophages in *Pik3cg*$^{-/-}$ HFD-fed mice. Because CD8$^+$ T cells have recently been reported to contribute to obesity-induced inflammation in adipose tissue and systemic insulin resistance (15), we assessed the *Cd8* expression level in the eWAT of HFD-fed mice and found a small and nonsignificant reduction in the eWAT of *Pik3cg*$^{-/-}$ mice (Fig. S4*C*), suggesting that deletion of PI3Kγ more prominently affected the infiltration of M1 macrophages. To gain additional insight into the clinical importance of PI3Kγ in the fat of obese subjects, we analyzed the expression of *PIK3CG* in s.c. adipose

tissue samples of humans with a wide range of values for body mass index (BMI) (16.4–32.0). Levels of *PIK3CG* expression showed a strong correlation with BMI ($P = 0.0009$) and also correlated with *ITGAX* expression levels ($P = 0.0087$) (Fig. S5).

ATMs have been identified as the major source of inflammatory cytokine/adipokine production in the adipose tissues of obese subjects, and these chemokines are thought to be a cause of chronic inflammation and systemic insulin resistance in obesity (3). Consistent with this idea, expression levels of *Tnf*, *Ccl2*, *Ccr2*, and *Nos2* in the eWAT of HFD-fed mice were increased, whereas these increases were significantly attenuated by PI3Kγ deletion (Fig. 2*I*). Furthermore, circulating monocyte chemotactic protein-1 (MCP-1) levels also decreased with a trend toward reductions in c-jun N-terminal kinase, and IκB kinase phosphorylation in the eWAT of *Pik3cg*$^{-/-}$ mice (Fig. 2*J* and Fig. S4 *E* and *F*). Taken together, these data suggest that the loss of PI3Kγ specifically suppresses M1 macrophage infiltration, leading to suppression of HFD-induced inflammation in adipose tissue, and finally leading to improved insulin sensitivity.

However, it remained possible that deficiency of PI3Kγ would modulate insulin sensitivity through other mechanisms. Indeed, we found that elevated leptin levels observed during HFD feeding were significantly decreased with a trend to decrease *Socs3* expression by deletion of PI3Kγ (Fig. S4 *G* and *H*), suggesting improved leptin sensitivity. This could be caused by reductions of proinflammatory adipokines and also through reduced macrophage infiltration in the hypothalamus by deletion of PI3Kγ, as evidenced by deceased expression of *Emr1* (Fig. S4*H*). However, the effect appeared very limited because food intake, energy expenditure, and genes regulated by leptin were not altered by deletion of PI3Kγ.

Loss of PI3Kγ Ameliorated Diet-Induced Hepatic Steatosis. Next, we assessed the impact of PI3Kγ deficiency on HFD-induced hepatic steatosis, which is known to be tightly associated with hepatic and systemic insulin resistance (16, 17). Interestingly, hepatic triglyceride content was significantly suppressed in the livers of *Pik3cg*$^{-/-}$ mice compared with that seen in *Pik3cg*$^{+/+}$ mice, which is consistent with the histological findings by hematoxylin and eosin (H&E) staining (Fig. 3*A* and *B*). Hepatic steatosis can be caused by overproduction of fatty acid, reduced fatty acid oxidation, increased lipid transport, and their combinations. Expression levels of genes involved in fatty acid synthesis tested here were not affected by PI3Kγ deletion (Fig. 3*C*, *Upper*), whereas *Cpt1a*, which involves fatty acid oxidation, was significantly increased in HFD-fed *Pik3cg*$^{-/-}$ mice compared with *Pik3cg*$^{+/+}$ mice (Fig. 3*C*, *Upper*). Intriguingly, expression of *Cidec* (encoding Fsp27) and *Cd36* in HFD-fed conditions was markedly suppressed in the livers of *Pik3cg*$^{-/-}$ mice (Fig. 3*C*, *Lower*). Expression of peroxisome proliferator-activated receptors (PPARγ), which is known to directly regulate *Cidec*, *Cd36*, *Scd1*, and *Pparg* itself (18–22), was also significantly decreased by deletion of PI3Kγ (Fig. 3*C*, *Lower*). Moreover, similar to findings seen with eWAT, expression of *Cd68*, *Tnf*, *Ccl2*, and its receptor *Ccr2* was significantly decreased in the livers of *Pik3cg*$^{-/-}$ mice compared with that seen in *Pik3cg*$^{+/+}$ mice (Fig. 3 *D* and *E*), and M2 macrophage markers (*Arg1*, *Mrc1*, *Mgl1*, and *Mgl2*) were up-regulated (Fig. 3*F*). The MCP-1/chemokine (C-C motif) receptor 2 (CCR2) pathway, which lies upstream of PI3Kγ, has been reported to contribute to the development of hepatic steatosis (6, 23, 24), and our findings may provide a missing link between hepatic steatosis and inflammation.

Loss of PI3Kγ in *ob/ob* Mice Reduced Inflammatory Changes in Adipose Tissue, Leading to Improvement of Insulin Sensitivity. To further assess the role of PI3Kγ in obesity-induced inflammation and insulin resistance, we generated *Pik3cg*$^{-/-}$ mice with a leptin-deficient background (*Pik3cg*$^{-/-}$*:ob/ob*). Although *Pik3cg*$^{-/-}$*:ob/ob* mice gained body weight in a similar manner compared with *Pik3cg*$^{+/+}$*:ob/ob* mice, they displayed lower blood glucose levels up to 20 wk of age (Fig.4 *A* and *B*). Similarly, *Pik3cg*$^{-/-}$*:ob/ob* mice also displayed significantly decreased glucose levels in a fasted state as well as during ITT and GTT (Fig. 4 *C* and *D*) along with enhanced insulin-stimulated Akt (also known as protein kinase B or PKB) phosphorylation in both liver and muscle

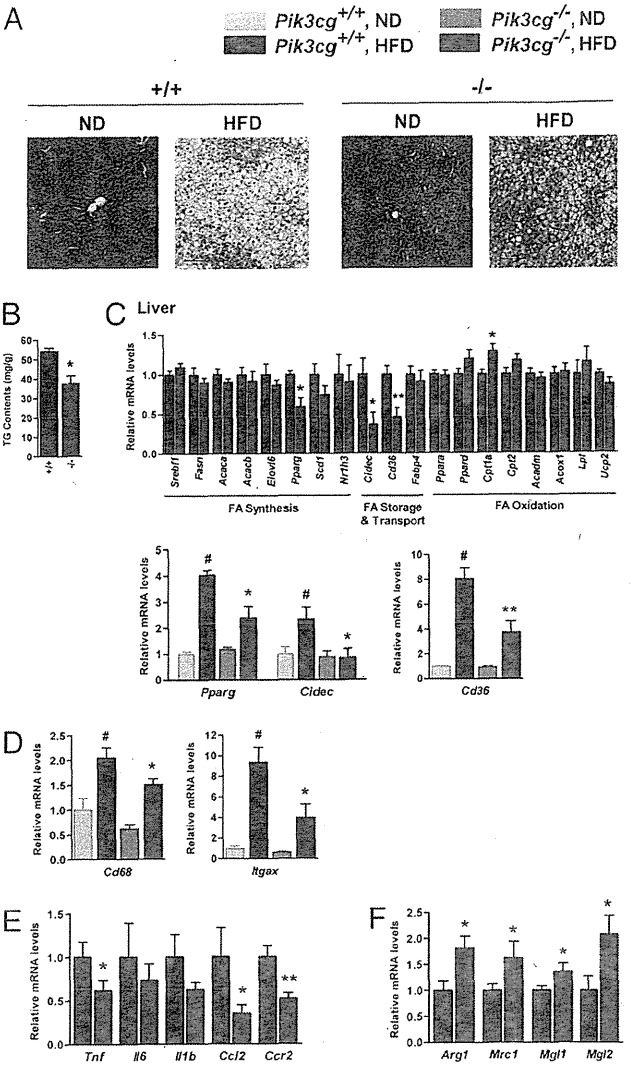

Fig. 3. PI3Kγ knockout mice showed amelioration of HFD-induced hepatic steatosis. (*A*) Hematoxylin and eosin-stained sections of liver from *Pik3cg*$^{+/+}$ ($^{+/+}$) and *Pik3cg*$^{-/-}$ ($^{-/-}$) mice on a ND or a HFD. (Scale bar, 100 μm.) (*B*) Triglyceride (TG) content in liver of mice on a HFD ($n = 7–8$). (*C*) Expression levels of mRNA related to fatty acid metabolism in liver of fasted mice ($n = 7–8$). (*D–F*) Expression levels of genes encoded macrophage-related protein (*D*), proinflammatory genes (*E*), and M2 macrophage-specific genes (normalized to *Cd68*, *F*) in liver ($n = 7–8$). #$P < 0.05$ for a HFD compared with ND. *$P < 0.05$ and **$P < 0.01$ for *Pik3cg*$^{-/-}$ mice compared with *Pik3cg*$^{+/+}$ controls.

of *Pik3cg*$^{-/-}$*:ob/ob* mice (Fig. 4*E*). In addition, the expression of *Emr1*, *Cd68*, and *Tnf* in the eWAT of *Pik3cg*$^{-/-}$*:ob/ob* mice was also significantly decreased (Fig. 4 *F* and *G*), whereas M2 macrophage markers were up-regulated (Fig. 4*H*). These data suggest that loss of PI3Kγ ameliorated obesity-induced insulin resistance through the reduction of macrophage infiltration and inflammation even in a genetically obese model and that a large part of these beneficial effects of PI3Kγ deficiency on glucose metabolism appears to be independent of leptin signaling and body weight change.

Bone Marrow-Specific Deletion of PI3Kγ Ameliorates Obesity-Induced Diabetes. Although PI3Kγ is almost exclusively expressed in hematopoietic cells, to rule out the possibility that PI3Kγ in extrahematopoietic parenchymal tissues might play some role in glucose metabolism, we generated a bone marrow (BM)-specific PI3Kγ deletion in *ob/ob* [*Pik3cg*$^{-/-}$ bone marrow transplant

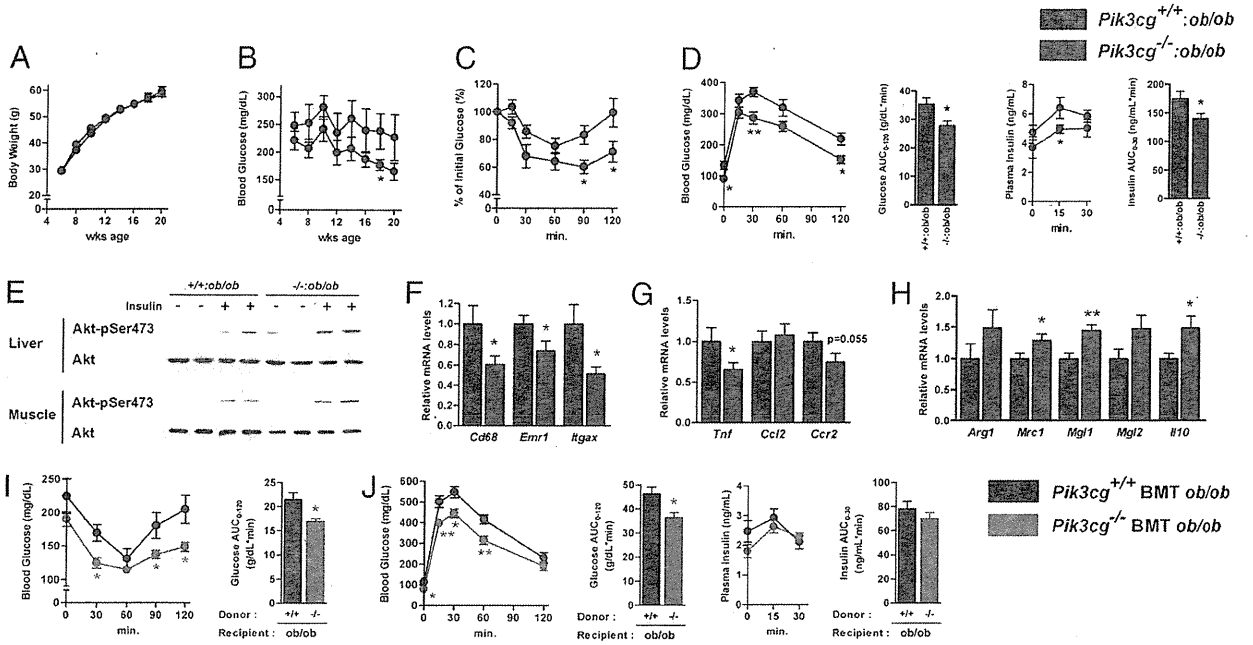

Fig. 4. Loss of PI3Kγ in the *ob/ob* background improved insulin sensitivity. (*A* and *B*) Time course of body weight (*A*) and blood glucose (*B*) in *Pik3cg*$^{+/+}$*:ob/ob* and double-mutant *Pik3cg*$^{-/-}$*:ob/ob* mice (n = 12–18). (*C*) Glucose levels during ITT (8 wk of age) were determined at the indicated time points after i.p. injection with a bolus of insulin (2.0 U·kg^{-1} BW) (n = 7–8). (*D*) Glucose and insulin levels during GTT (9 wk of age) were determined at the indicated time points after i.p. injection with a bolus of glucose (1.0 g·kg^{-1} BW) (n = 7–8). (*E*) Phosphorylation of Akt in livers and skeletal muscles induced by a bolus injection of insulin was assessed. (*F–H*) Expression levels of genes encoded macrophage-related protein (*F*), proinflammatory genes (*G*), and M2 macrophage-specific genes (normalized to *Cd68*, *H*) in eWAT (n = 7–8). (*I* and *J*) Bone marrow-specific PI3Kγ knockout *ob/ob* mice were generated by bone marrow transplantation. (*I*) Glucose levels during ITT were determined at the indicated time points after i.p. injection with a bolus of insulin (2.0 U·kg^{-1} BW). (*J*) Glucose and insulin levels during GTT were determined at the indicated time points after i.p. injection with a bolus of glucose (1.0 g·kg^{-1} BW) (n = 6). *P < 0.05, **P < 0.01.

(BMT) *ob/ob*] mice by BM transplantation. Compared with the control mice that received the *Pik3cg*$^{+/+}$ BM cells, *Pik3cg*$^{-/-}$ BMT *ob/ob* mice displayed improved glucose levels, systemic insulin sensitivity, and glucose intolerance (Fig. 4 *I* and *J*), as observed in *ob/ob* mice systemically lacking *Pik3cg*$^{-/-}$. These data strongly suggest that the metabolic phenotypes of *Pik3cg*$^{-/-}$*:ob/ob* mice are mainly owing to the lack of PI3Kγ in BM-derived cells. Moreover, we also confirmed that BM-specific *Pik3cg*$^{-/-}$ (*Pik3cg*$^{-/-}$ BMT) mice fed a HFD exhibited the phenotypes similar to those of mice systemically lacking *Pik3cg*$^{-/-}$ (Fig. S6). Furthermore, the in vitro studies revealed that lack of PI3Kγ did not significantly alter expression of *Itgax* in BM-derived macrophages (BMDM), induction of *Mgl2* in IL-4–stimulated alternative activation in BMDM, or LPS-stimulated proinflammatory cytokine expression in peritoneal macrophages (Fig. S7 *A–C*).

Blockade of PI3Kγ by a Pharmacological Inhibitor Ameliorated Obesity-Induced Diabetes. Finally, we addressed whether pharmacological inhibition of PI3Kγ could ameliorate insulin resistance in obese diabetic animal models using AS-605240, a small-molecule inhibitor for PI3Kγ (25). We confirmed that AS-605240 selectively blocked class IB PI3K signaling in cultured macrophages (Fig. S7*D*), as shown in the previous reports (26, 27). Treatment with 10 mg/kg/d of AS-605240 lowered blood glucose levels, with an associated significant improvement of both insulin sensitivity and glucose tolerance (Fig. 5 *A–C*) without affecting body weight (54.2 ± 0.8 g for vehicle, 54.0 ± 0.5 g for 10 mg/kg/d of AS-605240). A total of 30 mg/kg/d of AS-605240 displayed more profound effects (Fig. 5 *A–C*) with slightly less weight gain (49.5 ± 0.8 g). Moreover, AS-605240 dose-dependently reduced the abundance of ATMs as estimated by F4/80 staining and the expression levels of macrophage markers in eWAT (Fig. 5 *D* and *E*). As a consequence, the circulating levels of MCP-1 were also reduced in *ob/ob* mice treated with AS-605240 (Fig. 5*F*). We also confirmed that *Pik3cg*$^{+/+}$ mice fed a HFD treated with AS-605240 exhibited metabolic phenotypes very similar to those of *Pik3cg*$^{-/-}$ mice (Fig. S8). These findings strongly suggest that pharmacological intervention by inhibiting PI3Kγ is effective even after establishment of a morbidly obese condition.

Discussion

Obesity causes a variety of metabolic disorders, including diabetes and fatty liver disease, initiated by macrophage infiltration into adipose tissue and presumably also into liver. Previous studies have shown that MCP-1 triggers this macrophage infiltration and that modulation of the MCP-1/CCR2 signaling by genetic disruption or treatment with an inhibitory molecule can ameliorate obesity-induced insulin resistance (5, 6, 23, 24, 28). Other chemokines have recently been suggested to also promote macrophage infiltration in obesity (8, 29, 30). Receptors for these chemokines, including CCR2, are GPCRs, of which PI3Kγ lies downstream and mediates the signal to promote cell movement in response to chemokine stimulation (10, 11, 31, 32). Here, we show that suppression of PI3Kγ activity attenuates obesity-induced proinflammatory macrophage infiltration into adipose tissue and liver, leading to improvement of insulin resistance.

HFD feeding markedly increases CD11c-positive macrophages in eWAT as well as in the liver of *Pik3cg*$^{+/+}$ mice, whereas the increase is significantly suppressed by disruption of PI3Kγ. By contrast, the expression of the M2 macrophage marker is not decreased in these tissues of *Pik3cg*$^{-/-}$ mice fed a HFD, leading to an increase in the ratio of M2 to M1. This is because M1 macrophages, but not M2 macrophages, abundantly express CCR2 that promotes cell migration into both adipose tissue and liver via PI3Kγ activation. Furthermore, the results of BMT experiments using *ob/ob* or HFD-fed mice clearly demonstrate that the improved glucose metabolism caused by a lack of PI3Kγ is largely attributed to BM cells. Together with the results of in vitro experiments, the improved insulin sensitivity and glucose homeostasis associated with decreased inflammatory changes in the adipose tissue and liver of obese *Pik3cg*$^{-/-}$ mice

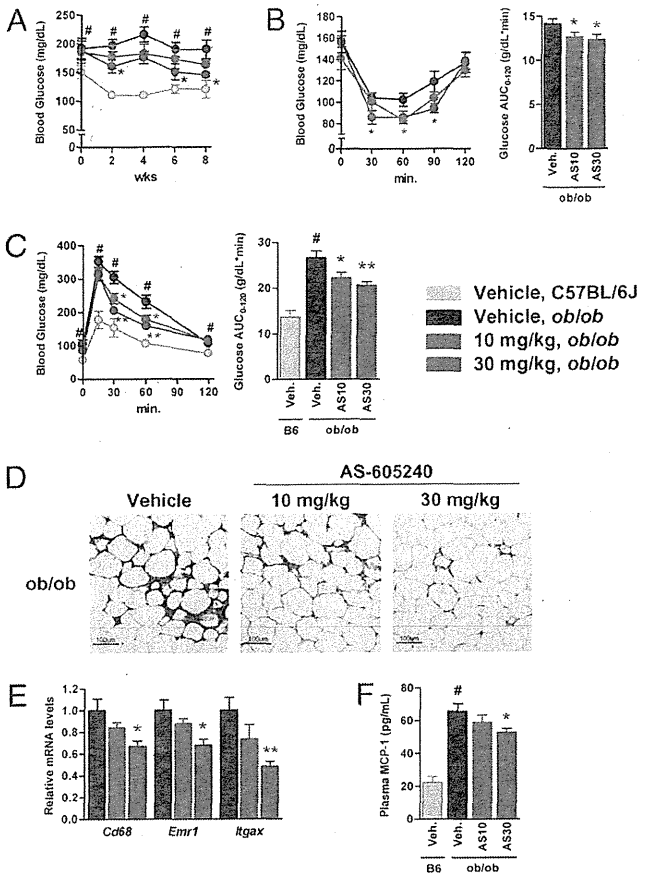

Fig. 5. Blockade of PI3Kγ by a pharmacological inhibitor ameliorated diabetes in *ob/ob* mice. *ob/ob* mice were treated with a PI3Kγ inhibitor, AS-605240, from 6 wk of age for 8 wk. Age-matched C57BL/6J mice served as lean controls. (*A*) Time course of blood glucose levels in vehicle, 10 or 30 mg/kg/d of AS-605240–treated *ob/ob* mice (designated as AS10 or AS30, respectively), and vehicle-treated C57BL/6J mice. (*B* and *C*) Glucose levels during ITT (7 wk treatment, *B*) or GTT (8 wk treatment, *C*) in vehicle (Veh.) or AS-605240–treated *ob/ob* mice were determined at the indicated time points after i.p. injection with a bolus of insulin (1.0 U·kg^{-1} BW) for ITT or glucose (1.5 g·kg^{-1} BW) for GTT. (*D*) Immunohistochemical analysis of adipose tissue macrophage. eWAT of *ob/ob* mice treated with vehicle or AS-605240 were stained with antibody against F4/80. (Scale bar, 100 μM.) (*E*) Expression levels of genes encoded macrophage-related protein in eWAT of vehicle or AS-605240–treated *ob/ob* mice. (*F*) Serum MCP-1 levels in vehicle or AS-605240–treated *ob/ob* mice and vehicle-treated C57BL/6J mice. (n = 7–8). #$P < 0.05$ for vehicle-treated *ob/ob* compared with vehicle-treated C57BL/6J mice. *$P < 0.05$ and **$P < 0.01$ for AS-605240–treated *ob/ob* compared with vehicle-treated *ob/ob* control.

are largely due to a reduction in the number of infiltrated M1 macrophages that produce proinflammatory adipokines, which thereby promotes systemic insulin resistance, but not the functional changes or differentiation defects in these cells.

Hepatic steatosis is also known to exacerbate insulin resistance in obesity and cause liver dysfunction, such as nonalcoholic steatohepatitis (33). In the liver of *Pik3cg*$^{-/-}$ mice, expression of *Pparg* and *Cidec* is significantly decreased without any alterations in genes involved in fatty acid synthesis, whereas genes regulating β-oxidation, such as *Cpt1a*, are up-regulated, consistent with the previous report that Fsp27 suppresses β-oxidation and triglyceride turnover in hepatocytes (21). Fsp27 has been reported to regulate lipid droplet formation downstream of PPARγ in adipocytes, and deletion of Fsp27 leads to protection from diet-induced obesity (22), although it is unclear whether Fsp27 also functions as a key regulator of lipid droplet formation in hepatocytes. Meanwhile, PPARγ expression levels in the eWAT of *Pik3cg*$^{-/-}$ mice are not suppressed differently from those in liver. It is proposed that, when the capacity of lipid storage in adipose tissue, presumably regulated by PPARγ, reaches a limit, accumulation of lipids in extra-adipose tissue, such as liver and muscle, takes place, leading to insulin resistance (1, 16). Moreover, it has been suggested that suppression of inflammation reduces the development of hepatic steatosis and insulin resistance. Indeed, treatment with a CCR2 inhibitor ameliorates insulin resistance and hepatic steatosis in *db/db* mice associated with significant reductions in the expression of CD36 in liver (23). Although it remains unclear how PI3Kγ deficiency causes the suppression of lipid accumulation in liver, it is possible that inhibition of macrophage infiltration into adipose tissue and liver, and the subsequent reduction of inflammatory changes, can decrease PPARγ expression in liver but not in adipocytes. This may inhibit the ectopic lipid accumulation, leading to systemic insulin sensitivity, although it should be explored how PPARγ is regulated in these tissues.

Inhibitors for PI3Kδ and PI3Kγ are expected to be therapeutic agents for chronic inflammatory diseases (34, 35). Indeed, pharmacological inhibition of PI3Kγ ameliorates rheumatoid arthritis, lupus nephritis, and atherosclerosis in mouse models (25, 27, 34, 36), and here we provide evidence that the PI3Kγ inhibition is also promising for treatment of obesity-induced diabetes. Because multiple chemokine-signaling pathways can be involved in macrophage infiltration and inflammation in an obese context, and because inhibition of PI3Kγ could suppress macrophage migration caused by all these chemokines (8, 34), blockade of PI3Kγ appears to have advantages compared with the strategies to inhibit single chemokine signaling, such as MCP-1 or CCR2, which have been shown to improve insulin sensitivity in obese mice (6, 23, 28). However, a highly selective inhibitor for PI3Kγ, which does not affect class IA PI3Ks and other kinases, should be developed and carefully evaluated for clinical use to avoid potential adverse effects, such as inhibition of insulin signaling. Nevertheless, our data suggest that PI3Kγ inhibition can be a strategy for treating obesity-induced insulin resistance.

We have clearly demonstrated that PI3Kγ plays a crucial role in obesity-induced inflammation, hepatic steatosis, and systemic insulin resistance and that inhibition of PI3Kγ activity ameliorates obesity-induced insulin resistance, at least in part, due to the reductions in macrophage infiltration and subsequent inflammatory responses in both adipose tissue and liver. These findings provide a possibility for a therapeutic approach to obesity-induced diabetes and fatty liver disease.

Materials and Methods

Mice. We generated *Pik3cg*$^{-/-}$ mice as previously described (11) and used these mice after they were backcrossed to C57BL/6J mice for more than 16 generations with C57BL/6J mice as the controls. *Pik3cg*$^{-/-}$:*ob/ob* mice were generated by intercrossing *Pik3cg*$^{+/-}$:*ob/+* mice. All mice were housed under a 12-h light/12-h dark cycle and had free access to sterile water and pellet food ad libitum except when fed a limited HFD. The animal care and experimental procedures were approved by the Animal Care Committee of the University of Tokyo.

Metabolic Studies. Male *Pik3cg*$^{-/-}$ and *Pik3cg*$^{+/+}$ mice were fed a standard chow (CE-2; CLEA Japan) or high-fat/high-caloric diet (high fat diet 32; CLEA Japan). For ITTs, mice received i.p. injections of human insulin (Humalin R; Eli Lilly) in the ad libitum feeding state. For GTTs, mice received i.p. injections of glucose after an overnight fast. Blood glucose levels were measured using a Glutest sensor (Sanwa Chemical) at the indicated time points, and the plasma insulin levels were measured using a RIA kit (Biotrek), as previously described (37).

Insulin-Signaling Analysis. Mice were anesthetized after 16 h of fasting, and human insulin was injected into the inferior vena cava. After 5 min, tissues were quickly excised and frozen in liquid nitrogen. Tissue lysates were prepared and used for immunoprecipitation and immunoblotting as previously described (38).

Gene Expression Analysis. TRIzol reagent (Invitrogen) was used to prepare total RNA from tissues. The reverse-transcription reaction was carried out with a high-capacity cDNA reverse transcription kit (Applied Biosystems). Quantitative PCR analyses using TaqMan assays were performed as previously described (37). The relative expression levels were normalized by measurement of the amount of cyclophilin in each sample.

Histological Analysis. Tissue samples for histology were fixed in 4% paraformaldehyde in PBS overnight, and paraffin-embedded sections were prepared (4-μm sections). Sections of liver were stained with H&E, and adipose tissues were stained hematoxylin and incubated with anti-F4/80 (1:20; Serotec) overnight at 4 °C, followed by incubation with the Vectastain Elite ABC Rat IgG Kit and visualization with the ImmPACT DAB Substrate Kit (Vector Laboratories), as previously described (5).

Adipose Tissue Fractionation and FACS Analysis. Adipose tissue fractionation into the stromal vascular fraction (SVF) was performed as previously described (5). Briefly, epididymal adipose tissue pads were minced into fine pieces and centrifuged at 3,000 × *g* to remove erythrocytes and free leukocytes. Tissues were incubated with 2 mg/mL of collagenase type 2 (Worthington) at 37 °C with gentle agitation for 15–20 min. Digested tissues were filtered through nylon mesh (100 μm), and the filtrate was centrifuged at 1,200 × *g*. Pelleted cells were collected as the SVF. For isolation of mRNA, the erythrocyte-depleted SVF was resuspended in TRIzol reagent (Invitrogen). For flow cytometric analysis, after removing red blood cells, the SVF was incubated with either labeled monoclonal antibody or isotype control antibody and analyzed by flow cytometry using a FACS Calibur (Becton Dickinson). Data acquisition and analysis were performed using CellQuest Pro software (Becton Dickinson). Propidium iodide was used to exclude dead cells.

Plasma MCP-1 and Hepatic Triglyceride Content. Plasma levels for MCP-1 were measured by ELISA (R&D Systems). Hepatic triglyceride was extracted from the liver homogenate with Folchsolutioin (chloroform:methanol = 2:1, vol/vol). An aliquot of the organic phase was collected and resuspended in ethanol containing 1% Triton X-100 and then measured by enzyme-based measurement kits (Roche Diagnostics).

Bone Marrow Transplantation. For BM transplant studies, bone marrow cells were prepared from the femur and tibia of *Pik3cg*$^{+/+}$ and *Pik3cg*$^{-/-}$ mice and injected i.v. (5 × 10^6 cells/recipient) into lethally irradiated *ob/ob* mice or C57BL/6J mice (7.0 Gy) as recipients, as described previously (39, 40).

Treatment with a PI3Kγ Inhibitor. A PI3Kγ selective inhibitor, AS-605240, which was synthesized by Discovery Research Laboratories, Kyorin Pharmaceutical, was used as described previously (25). Vehicle or AS-605240 was administered intraperitoneally to *ob/ob* mice twice a day from 6 wk of age.

Statistical Analysis. Values of the data are expressed as mean ± SEM. Differences between two groups were assessed using unpaired two-tailed *t* tests. Data involving more than two groups were assessed by analysis of variance. Statistical significance is displayed as $P < 0.05$ (one asterisk) or $P < 0.01$ (two asterisks) in figures.

ACKNOWLEDGMENTS. We thank R. Hoshino, F. Takahashi, Y. Kanto, and Y. Kishida for their excellent technical assistance. This work was supported by a grant for the Translational Systems Biology and Medicine Initiative from the Ministry of Education, Culture, Sports, Science and Technology of Japan (to T.K.), a Grant-in-Aid for Scientific Research in Priority Areas (S) from the Ministry of Education, Culture, Sports, Science and Technology of Japan (to T.K.), a Grant-in-Aid for Scientific Research in Priority Areas (B) from the Ministry of Education, Culture, Sports, Science and Technology of Japan (to K.U.), a Grant-in-Aid for Scientific Research from the Ministry of Health, Labor and Welfare (to K.U.), Health Science Research grants (Research on Human Genome and Gene Therapy) from the Ministry of Health and Welfare (to T.K.), and a grant from Takeda Science Foundation (to K.U.).

1. Kahn SE, Hull RL, Utzschneider KM (2006) Mechanisms linking obesity to insulin resistance and type 2 diabetes. *Nature* 444:840–846.
2. Yach D, Stuckler D, Brownell KD (2006) Epidemiologic and economic consequences of the global epidemics of obesity and diabetes. *Nat Med* 12:62–66.
3. Weisberg SP, et al. (2003) Obesity is associated with macrophage accumulation in adipose tissue. *J Clin Invest* 112:1796–1808.
4. Xu H, et al. (2003) Chronic inflammation in fat plays a crucial role in the development of obesity-related insulin resistance. *J Clin Invest* 112:1821–1830.
5. Kamei N, et al. (2006) Overexpression of monocyte chemoattractant protein-1 in adipose tissues causes macrophage recruitment and insulin resistance. *J Biol Chem* 281:26602–26614.
6. Kanda H, et al. (2006) MCP-1 contributes to macrophage infiltration into adipose tissue, insulin resistance, and hepatic steatosis in obesity. *J Clin Invest* 116:1494–1505.
7. Zeyda M, et al. (2007) Human adipose tissue macrophages are of an anti-inflammatory phenotype but capable of excessive pro-inflammatory mediator production. *Int J Obes (Lond)* 31:1420–1428.
8. Chavey C, et al. (2009) CXC ligand 5 is an adipose-tissue derived factor that links obesity to insulin resistance. *Cell Metab* 9:339–349.
9. Oak JS, Matheu MP, Parker I, Cahalan MD, Fruman DA (2007) Lymphocyte cell motility: The twisting, turning tale of phosphoinositide 3-kinase. *Biochem Soc Trans* 35:1109–1113.
10. Hirsch E, et al. (2000) Central role for G protein-coupled phosphoinositide 3-kinase gamma in inflammation. *Science* 287:1049–1053.
11. Sasaki T, et al. (2000) Function of PI3Kgamma in thymocyte development, T cell activation, and neutrophil migration. *Science* 287:1040–1046.
12. Lumeng CN, Bodzin JL, Saltiel AR (2007) Obesity induces a phenotypic switch in adipose tissue macrophage polarization. *J Clin Invest* 117:175–184.
13. Lumeng CN, DelProposto JB, Westcott DJ, Saltiel AR (2008) Phenotypic switching of adipose tissue macrophages with obesity is generated by spatiotemporal differences in macrophage subtypes. *Diabetes* 57:3239–3246.
14. Gordon S (2003) Alternative activation of macrophages. *Nat Rev Immunol* 3:23–35.
15. Nishimura S, et al. (2009) CD8+ effector T cells contribute to macrophage recruitment and adipose tissue inflammation in obesity. *Nat Med* 15:914–920.
16. Després JP, Lemieux I (2006) Abdominal obesity and metabolic syndrome. *Nature* 444: 881–887.
17. Perlemuter G, Bigorgne A, Cassard-Doulcier AM, Naveau S (2007) Nonalcoholic fatty liver disease: From pathogenesis to patient care. *Nat Clin Pract Endocrinol Metab* 3: 458–469.
18. Tontonoz P, Spiegelman BM (2008) Fat and beyond: The diverse biology of PPARgamma. *Annu Rev Biochem* 77:289–312.
19. Bouhlel MA, et al. (2007) PPARgamma activation primes human monocytes into alternative M2 macrophages with anti-inflammatory properties. *Cell Metab* 6: 137–143.
20. Odegaard JI, et al. (2007) Macrophage-specific PPARgamma controls alternative activation and improves insulin resistance. *Nature* 447:1116–1120.
21. Matsusue K, et al. (2008) Hepatic steatosis in leptin-deficient mice is promoted by the PPARgamma target gene Fsp27. *Cell Metab* 7:302–311.
22. Nishino N, et al. (2008) FSP27 contributes to efficient energy storage in murine white adipocytes by promoting the formation of unilocular lipid droplets. *J Clin Invest* 118: 2808–2821.
23. Tamura Y, et al. (2008) Inhibition of CCR2 ameliorates insulin resistance and hepatic steatosis in db/db mice. *Arterioscler Thromb Vasc Biol* 28:2195–2201.
24. Yang SJ, Iglayreger HB, Kadouh HC, Bodary PF (2009) Inhibition of the chemokine (C-C motif) ligand 2/chemokine (C-C motif) receptor 2 pathway attenuates hyperglycaemia and inflammation in a mouse model of hepatic steatosis and lipoatrophy. *Diabetologia* 52:972–981.
25. Barber DF, et al. (2005) PI3Kgamma inhibition blocks glomerulonephritis and extends lifespan in a mouse model of systemic lupus. *Nat Med* 11:933–935.
26. Guillermet-Guibert J, et al. (2008) The p110beta isoform of phosphoinositide 3-kinase signals downstream of G protein-coupled receptors and is functionally redundant with p110gamma. *Proc Natl Acad Sci USA* 105:8292–8297.
27. Camps M, et al. (2005) Blockade of PI3Kgamma suppresses joint inflammation and damage in mouse models of rheumatoid arthritis. *Nat Med* 11:936–943.
28. Weisberg SP, et al. (2006) CCR2 modulates inflammatory and metabolic effects of high-fat feeding. *J Clin Invest* 116:115–124.
29. Huber J, et al. (2008) CC chemokine and CC chemokine receptor profiles in visceral and subcutaneous adipose tissue are altered in human obesity. *J Clin Endocrinol Metab* 93:3215–3221.
30. Nara N, et al. (2007) Disruption of CXC motif chemokine ligand-14 in mice ameliorates obesity-induced insulin resistance. *J Biol Chem* 282:30794–30803.
31. Ferguson GJ, et al. (2007) PI(3)Kgamma has an important context-dependent role in neutrophil chemokinesis. *Nat Cell Biol* 9:86–91.
32. Nishio M, et al. (2007) Control of cell polarity and motility by the PtdIns(3,4,5)P3 phosphatase SHIP1. *Nat Cell Biol* 9:36–44.
33. Nugent C, Younossi ZM (2007) Evaluation and management of obesity-related nonalcoholic fatty liver disease. *Nat Clin Pract Gastroenterol Hepatol* 4:432–441.
34. Rückle T, Schwarz MK, Rommel C (2006) PI3Kgamma inhibition: Towards an 'aspirin of the 21st century'? *Nat Rev Drug Discov* 5:903–918.
35. Marone R, Cmiljanovic V, Giese B, Wymann MP (2008) Targeting phosphoinositide 3-kinase: Moving towards therapy. *Biochim Biophys Acta* 1784:159–185.
36. Chang JD, et al. (2007) Deletion of the phosphoinositide 3-kinase p110gamma gene attenuates murine atherosclerosis. *Proc Natl Acad Sci USA* 104:8077–8082.
37. Kubota N, et al. (2008) Dynamic functional relay between insulin receptor substrate 1 and 2 in hepatic insulin signaling during fasting and feeding. *Cell Metab* 8:49–64.
38. Ueki K, et al. (2002) Increased insulin sensitivity in mice lacking p85β subunit of phosphoinositide 3-kinase. *Proc Natl Acad Sci USA* 99:419–424.
39. Goyama S, et al. (2008) Evi-1 is a critical regulator for hematopoietic stem cells and transformed leukemic cells. *Cell Stem Cell* 3:207–220.
40. Ito A, et al. (2008) Role of CC chemokine receptor 2 in bone marrow cells in the recruitment of macrophages into obese adipose tissue. *J Biol Chem* 283: 35715–35723.

Cell Metabolism

Adiponectin Enhances Insulin Sensitivity by Increasing Hepatic IRS-2 Expression via a Macrophage-Derived IL-6-Dependent Pathway

Motoharu Awazawa,[1] Kohjiro Ueki,[1,2,*] Kazunori Inabe,[1] Toshimasa Yamauchi,[1] Naoto Kubota,[1,2,3] Kazuma Kaneko,[1] Masatoshi Kobayashi,[1] Aya Iwane,[1] Takayoshi Sasako,[1] Yukiko Okazaki,[1] Mitsuru Ohsugi,[1] Iseki Takamoto,[1] Satoshi Yamashita,[4] Hiroshi Asahara,[4] Shizuo Akira,[5] Masato Kasuga,[6] and Takashi Kadowaki[1,2,*]

[1]Department of Diabetes and Metabolic Diseases, Graduate School of Medicine, University of Tokyo, Tokyo 113-8655, Japan
[2]Translational Systems Biology and Medicine Initiative (TSBMI), University of Tokyo, Tokyo 113-8655, Japan
[3]Clinical Nutrition Program, National Institute of Health and Nutrition, Tokyo 162-8636, Japan
[4]Department of Systems BioMedicine, National Research Institute of Child Health and Development, Tokyo 157-8535, Japan
[5]Laboratory of Host Defense, WPI Immunology Frontier Research Center, Osaka University, Osaka 565-0871, Japan
[6]Research Institute, International Medical Center of Japan, Tokyo 162-0052, Japan
*Correspondence: ueki-tky@umin.ac.jp (K.U.), kadowaki-3im@h.u-tokyo.ac.jp (T.K.)
DOI 10.1016/j.cmet.2011.02.010

SUMMARY

Insulin resistance is often associated with impeded insulin signaling due either to decreased concentrations or functional modifications of crucial signaling molecules including insulin receptor substrates (IRS) in the liver. Many actions of adiponectin, a well-recognized antidiabetic adipokine, are currently attributed to the activation of two critical molecules downstream of AdipoR1 and R2: AMP-activated kinase (AMPK) and peroxisome proliferator-activated receptor α (PPARα). However, the direct effects of adiponectin on insulin signaling molecules remain poorly understood. We show here that adiponectin upregulates IRS-2 through activation of signal transducer and activator of transcription-3 (STAT3). Surprisingly, this activation is associated with IL-6 production from macrophages induced by adiponectin through NFκB activation independent of its authentic receptors, AdipoR1 and AdipoR2. These data have unraveled an insulin-sensitizing action initiated by adiponectin leading to upregulation of hepatic IRS-2 via an IL-6 dependent pathway through a still unidentified adiponectin receptor.

INTRODUCTION

Insulin resistance is often caused by decreased levels of its critical signaling molecules, functional modifications of these proteins, or both (Hotamisligil et al., 1996; Taniguchi et al., 2006). IRS-1 and IRS-2 are abundant in liver and are essential regulators for glucose metabolism in physiological and pathological circumstances (Dong et al., 2006; Kubota et al., 2008; Sun et al., 1995; Tamemoto et al., 1994). IRS-2 expression is preferentially decreased in the livers of obese model mice (Shimomura et al., 2000), and disruption of hepatic IRS-2 leads to insulin resistance (Kubota et al., 2000), suggesting that hepatic IRS-2 as well as IRS-1 is critical for the pathogenesis of systemic insulin resistance.

Adiponectin is an antidiabetic adipokine (Kadowaki et al., 2006), which enhances insulin action by several mechanisms, including suppression of gluconeogenesis and regulation of fatty acid metabolism (Awazawa et al., 2009; Berg et al., 2001; Yamauchi et al., 2001) as well as modulation of calcium signaling in skeletal muscles (Iwabu et al., 2010). To date, most of these actions have been attributed to the activation of two critical molecules downstream of AdipoR1 and AdipoR2, AMPK, and PPARα (Iwabu et al., 2010; Yamauchi et al., 2002; Yamauchi et al., 2007). In obese model mice with insulin resistance, hypoadiponectinemia (Yamauchi et al., 2001) often coexists with downregulation of hepatic insulin signaling; however, direct effects of adiponectin on insulin signaling molecules remain poorly investigated.

IL-6 is an inflammatory cytokine that has usually been related to insulin resistance, although some reports have paradoxically suggested that transient IL-6 upregulation contributes to improved insulin sensitivity (for a comprehensive review, see Pedersen and Febbraio, 2008). In contrast, adiponectin has been reported to exert anti-inflammatory actions (Huang et al., 2008), although it activates NFκB and induces inflammatory cytokines in some contexts (Haugen and Drevon, 2007). It is not precisely understood how adiponectin is related to inflammatory responses and cytokine production, including that of IL-6.

In this report, we show that adiponectin upregulates the IRS-2 protein thorough activation of STAT3 associated with IL-6 production from macrophages, independently of its authentic receptors, AdipoR1 and AdipoR2. These data have unraveled a novel adiponectin biology including the existence of an unidentified receptor.

RESULTS

IRS-2 Expression Was Decreased in Livers of Adiponectin-Deficient Mice, and Adiponectin Administration Upregulated IRS-2 in Liver

To examine the direct effects of adiponectin on insulin signaling, we first investigated the expression of insulin signaling

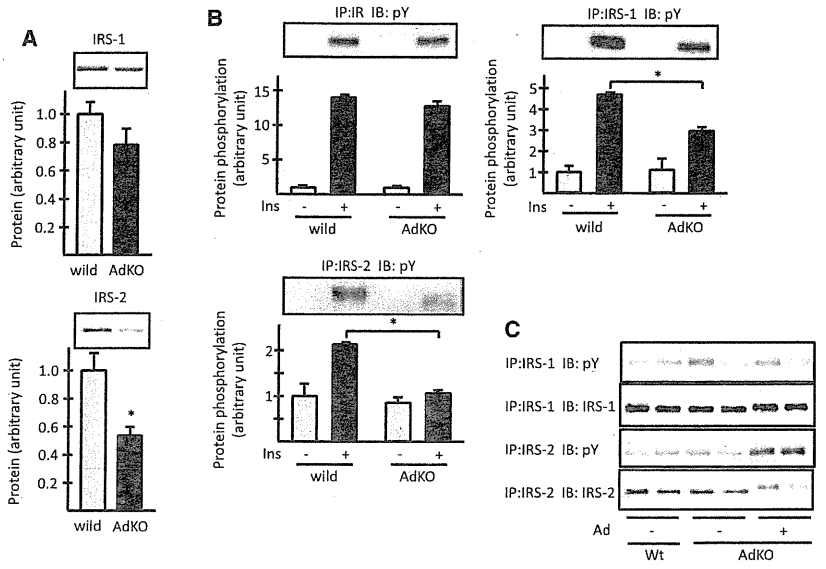

Figure 1. IRS-2 Expression Was Decreased in the Livers of Ad KO Mice

The representative blots of IRS-1 and IRS-2 in the livers of Ad KO mice and their arbitrary quantifications.

(A) Ad KO mice were sacrificed at the fasted state and the liver lysates were immunoprecipitated and immunoblotted with each antibody ($n = 4$, * $p < 0.05$).

(B) Ad KO mice were injected with insulin (Ins) and the livers were removed at 5 min. The lysates were immunoprecipitated with insulin receptor (IR), IRS-1, and IRS-2 antibody, respectively, and immunoblotted with 4G10 anti-phosphotyrosine (pY) antibody ($n = 4$, * $p < 0.05$).

(C) Ad KO mice were injected with adiponectin (Ad) intraperitoneally and the livers were removed at 4 hr. The lysates were immunoprecipitated with IRS-1 and IRS-2 antibody, respectively, and immunoblotted with pY, IRS-1 and IRS-2 antibody.

Error bars represent mean ± standard error of the mean (SEM).

molecules in the livers of adiponectin-deficient (AdKO) mice. The western blot revealed that IRS-2 protein levels were decreased in the livers of AdKO mice (Figure 1A), and IRS-2 phosphorylation by insulin was reduced (Figure 1B), while IRS-1 protein expression and its phosphorylation by insulin were relatively unaltered. Adiponectin administration in AdKO mice upregulated IRS-2 phosphorylation associated with its protein upregulation in liver (Figure 1C). These results prompted us to examine the possibility that adiponectin regulated IRS-2 expression in liver.

Adiponectin Upregulated IRS-2 and Restored Insulin Action in Livers of *db/db* Mice

We then administered adiponectin to *db/db* mice, an obese animal model with insulin resistance and selective downregulation of IRS-2 in the liver (Shimomura et al., 2000). Adiponectin administration, which raised the plasma concentration of adiponectin twice as high as preadministration levels (Figure S1A available online), restored hepatic IRS-2 protein and its phosphorylation (Figure 2A). This led to the recruitment of an adaptor molecule, the regulatory p85 subunit of phosphoinositide-3 (PI3) kinase, as assessed by the coimmunoprecipitation of IRS-2 and p85. In contrast, the expression and phosphorylation of insulin receptor (IR) and IRS-1 were unaltered with adiponectin administration (Figure 2A). Insulin stimulation after 4 hr of pretreatment with adiponectin showed partial but significant restoration of the impaired insulin signaling in livers of *db/db* mice, as evidenced by Akt and forkhead transcription factor FoxO1 phosphorylation, accompanied by IRS-2 upregulation (Figure 2B) and enhanced PI3 kinase activity associated with IRS-2 (Figure 2C), while IRS-1 phosphorylation and the PI-3 kinase activity associated with IRS-1 were unaltered. We also confirmed that adiponectin restored the downregulated IRS-2 and led to enhanced insulin signaling in high fat diet-induced obese mice (Figures S1B and S1C). These results indicated that adiponectin restored the attenuated insulin actions in liver of obese model mice via IRS-2 upregulation.

Time course experiments showed that adiponectin robustly upregulated hepatic *Irs2* messenger RNA (mRNA) at 2 hr (Figure 2D) and transiently and maximally increased IRS-2 protein at 4 hr (data nor shown). Importantly, adiponectin administration to *db/db* mice did not alter plasma glucose and insulin levels during 0.5–2 hr (data not shown), indicating that the changes in IRS-2 expression were the primary effects of adiponectin but not the consequence of altered plasma glucose or insulin levels, which could secondarily modulate IRS-2 expression. Moreover, adiponectin administration also increased IRS-2 protein in the livers of wild-type mice (Figure S1D).

The enhanced insulin signaling by adiponectin in the livers of *db/db* mice was associated with suppressed mRNA expressions of key gluconeogenic enzymes, phosphoenolpyruvate carboxykinase (*Pck1*) and glucose-6-phosphatase (*G6pc*) (Figure S1E) and led to lower plasma glucose concentrations in a pyruvate tolerance test (Figure S1F), suggesting that adiponectin administration suppressed gluconeogenesis in liver. In addition, adiponectin decreased the mRNA expression of sterol regulatory element binding protein 1c (*Srebf1*). Hepatic de novo lipogenesis, as assessed by ^{3}H and ^{14}C incorporation into saponified triglyceride, also tended to be lower in adiponectin-treated *db/db* mice (Figure S1G and Figure S1H).

Adiponectin Activated STAT3 in Liver, which Was Associated with Elevated Plasma IL-6 Concentration

Previously, we identified AdipoR1 and R2 as the receptors for adiponectin, both of which are abundant in the liver (Yamauchi et al., 2003), while T-cadherin, another possible receptor for adiponectin, is abundant in the cardiovascular system (Hug et al., 2004). We therefore hypothesized that adiponectin regulated IRS-2 expression directly through AdipoR1 or R2 in the liver. However, knockdown of neither AdipoR1 nor R2 in the liver attenuated *Irs2* upregulation by adiponectin (Figures S2A and

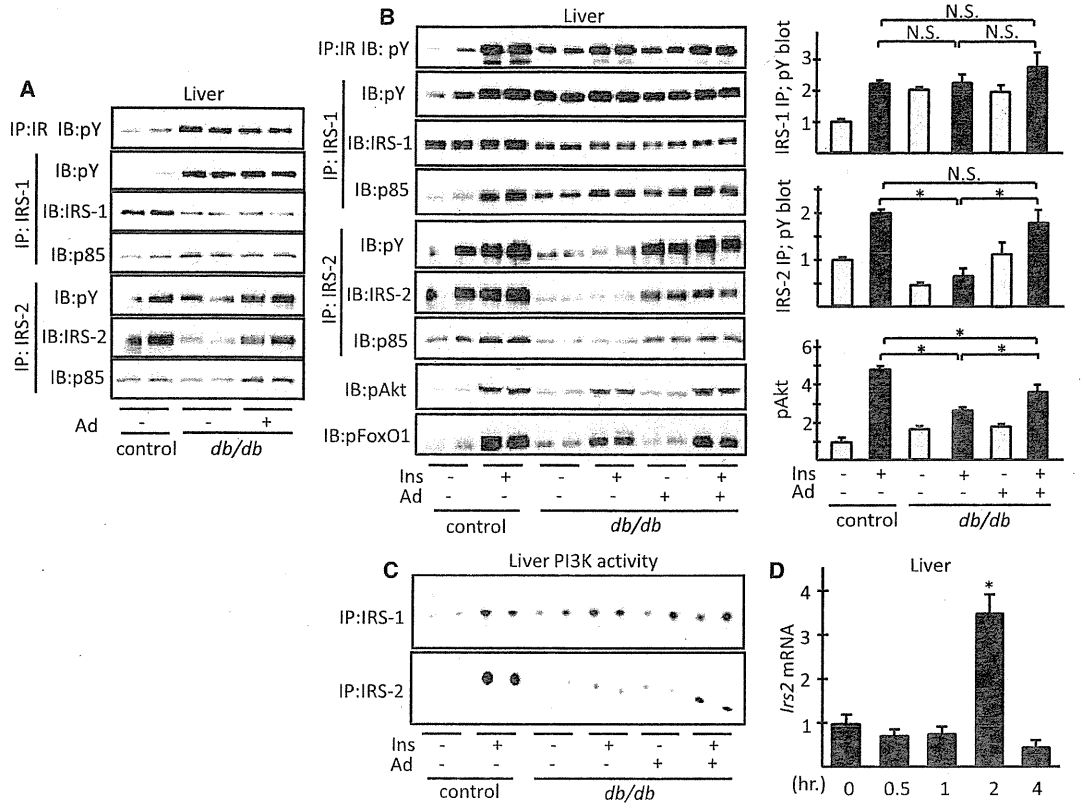

Figure 2. Adiponectin Upregulated IRS-2 Expression in the Liver of *db/db* Mice

(A–C) The representative blots of insulin signaling in the liver of *db/db* mice administered with adiponectin.

(A) *db/db* mice and their control *misty/misty* mice were injected with adiponectin (Ad) at the fasted state, and the livers were removed at 4 hr. The lysates were immunoprecipitated with insulin receptor (IR), IRS-1, and IRS-2 antibody, respectively, and were subjected to immunoblotting with 4G10 anti-phosphotyrosine (pY), IRS-1, IRS-2, and p85 subunit of PI3Kinase (p85) antibody.

(B) *db/db* mice and their control *misty/misty* mice were administered with Ad at the fasted state, and after 4 hr the mice were injected with insulin (Ins) via inferior venae cavae. The livers were removed at 5 min, except for phospho-FoxO1 blotting, for which the livers were removed at 2 min. The lysates were immunoprecipitated with IR, IRS-1, and IRS-2 antibody, respectively, and were subjected to immunoblotting with pY, IRS-1, IRS-2, p85, pAkt, and pFoxO1 antibody. The arbitrary quantifications are shown in the right-hand panels (n = 6, *; $p < 0.05$).

(C) *db/db* mice and their control *misty/misty* mice were injected with Ad at the fasted state, and after 4 hr the mice were injected with insulin (Ins) via inferior venae cavae. The livers were removed at 2 min and subjected to PI3 kinase assay as described in the Experimental Procedures.

(D) RT-PCR analysis of *Irs2* mRNA in the liver of *db/db* mice at indicated hours after Ad administration (n = 4, * $p < 0.05$).

Error bars represent mean ± SEM. See also Figure S1.

S2B). Furthermore, adiponectin stimulation did not upregulate *Irs2* in cultured hepatocytes (Figure S2C). These data raised the possibility that adiponectin indirectly upregulated hepatic IRS-2 through a previously unknown pathway.

To determine the mechanism of IRS-2 upregulation by adiponectin, we examined the changes in various signaling molecules in the liver after adiponectin administration, including those that had not been reported to regulate IRS-2. Of these, we noted strong phosphorylation of STAT3 in liver (Figure 3A). The time course in which the expression of the suppressor of cytokine signaling-3 (*Socs3*), the well-known downstream molecule of STAT3, was upregulated was almost identical with the time course in which *Irs2* was upregulated (Figure 3B), suggesting that *Irs2* and *Socs3* were upregulated by common upstream signaling(s). As expected, adiponectin stimulation of Fao cells did not cause STAT3 phosphorylation (Figure 3C). From these data, we had an assumption that adiponectin induced some biological substances in the plasma, which then induced hepatic STAT3 phosphorylation and IRS-2 expression secondarily, although it had not been reported that STAT3 directly regulated IRS-2 expression.

Surprisingly indeed, we found that adiponectin administration caused an acute and transient increase of plasma IL-6, a potent activator of STAT3 (Figure 3D), the time course of which was coincident with the STAT3 phosphorylation in liver. *Il6* mRNA was strongly upregulated in white adipose tissue (WAT) after adiponectin administration, while the *Il6* mRNA in liver was also upregulated to a much lesser extent (Figure 3E, left panel). Further analysis revealed that *Il6* induction was more prominent in visceral WAT than in subcutaneous WAT, with the

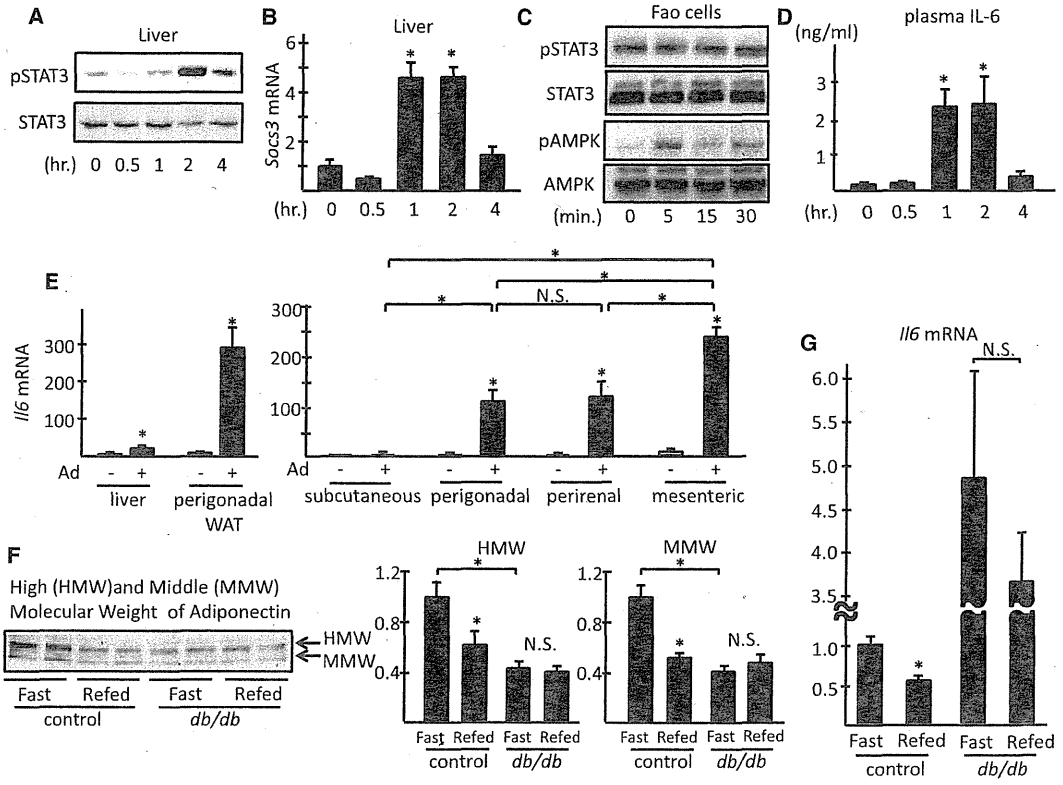

Figure 3. Hepatic STAT3 activation and IL-6 Induction after Adiponectin Administration

(A and B) The representative blot of pSTAT3/STAT3 (A) and RT-PCR analysis of *Socs3* mRNA (B) in the liver of *db/db* mice after adiponectin administration. *db/db* mice were injected with adiponectin (Ad) at the fasted state, and the livers were removed at the indicated hours. The lysates were immunoprecipitated with anti-STAT3 antibody and subjected to immunoblotting with pSTAT3 or STAT3 antibody. The total mRNA extracted from the livers was subjected to RT-PCR analysis ($n = 7$-12, * $p < 0.05$).

(C) The representative blots of pSTAT3/ STAT3 and pAMPK/AMPK in Fao cells stimulated with Ad. Fao cells were stimulated with Ad at indicated time, and the lysates were immunoprecipitated with anti-STAT3 antibody and subjected to immunoblotting with pSTAT3 or STAT3 antibody. The total cell lysates were subjected to western blotting with pAMPK and AMPK antibody.

(D) The plasma IL-6 concentration after adiponectin administration. *db/db* mice were injected with Ad at the fasted state. The plasma collected at indicated hours was subjected to ELISA assay ($n = 7$-12, * $p < 0.05$).

(E) RT-PCR analysis of *Il6* mRNA in liver and various WAT depots. *db/db* mice were injected with Ad at the fasted state, and the livers and the adipose tissues were removed at 2 hr. The total mRNA was extracted and subjected to RT-PCR analysis ($n = 5$-7, * $p < 0.05$).

(F) The representative blot of the diurnal changes in plasma adiponectin concentrations and their arbitrary quantification. The blood samples of *db/db* and their control *misty/misty* mice collected at the fasted or refed state were subjected to immunoblotting with anti-adiponectin antibody ($n = 4$, * $p < 0.05$).

(G) The diurnal changes of *Il6* mRNA expression in perigonadal WAT. *db/db* and their control *misty/misty* mice were sacrificed at the fasted and refed state. The total mRNA was extracted from the perigonadal WAT and subjected to RT-PCR analysis ($n = 4$-5, * $p < 0.05$).

Error bars represent mean ± SEM. See also Figure S2.

highest induction observed in mesenteric WAT (Figure 3E, right panel).

These data prompted us to hypothesize that adiponectin induced IL-6, which then activated hepatic STAT3 and subsequently upregulated IRS-2. Importantly, IRS-2 expression physiologically increases during fasting, and its function is crucial in the fasted state (Kubota et al., 2008). Indeed, consistent with our hypothesis, *Il6* expression was upregulated in the fasted state in WAT of wild-type mice and was associated with increased plasma adiponectin levels (Figures 3F and 3G). In contrast, *Il6* expression was highly and persistently upregulated in *db/db* mice with continuous downregulation of plasma adiponectin levels, regardless of the feeding state (Figures 3F and 3G).

IRS-2 Upregulation by Adiponectin was Mediated by Hepatic STAT3 Activation via IL-6

To verify our hypothesis, we first abrogated IL-6 action either by using neutralizing antibody or through genetic ablation (IL-6 knockout [KO] mice). Antibody-mediated IL-6 neutralization significantly attenuated hepatic STAT3 phosphorylation by adiponectin and abrogated the adiponectin-induced *Irs2* upregulation despite robust *Il6* induction (Figure 4A), which was confirmed by mRNA expression in perigonadal WAT. Moreover, in IL-6 KO mice, adiponectin-induced STAT3 phosphorylation and *Irs2* upregulation were totally abolished (Figure 4B).

In contrast, IL-6 administration upregulated *Irs2* mRNA and its phosphorylation in liver (Figure 4C) after phosphorylation of

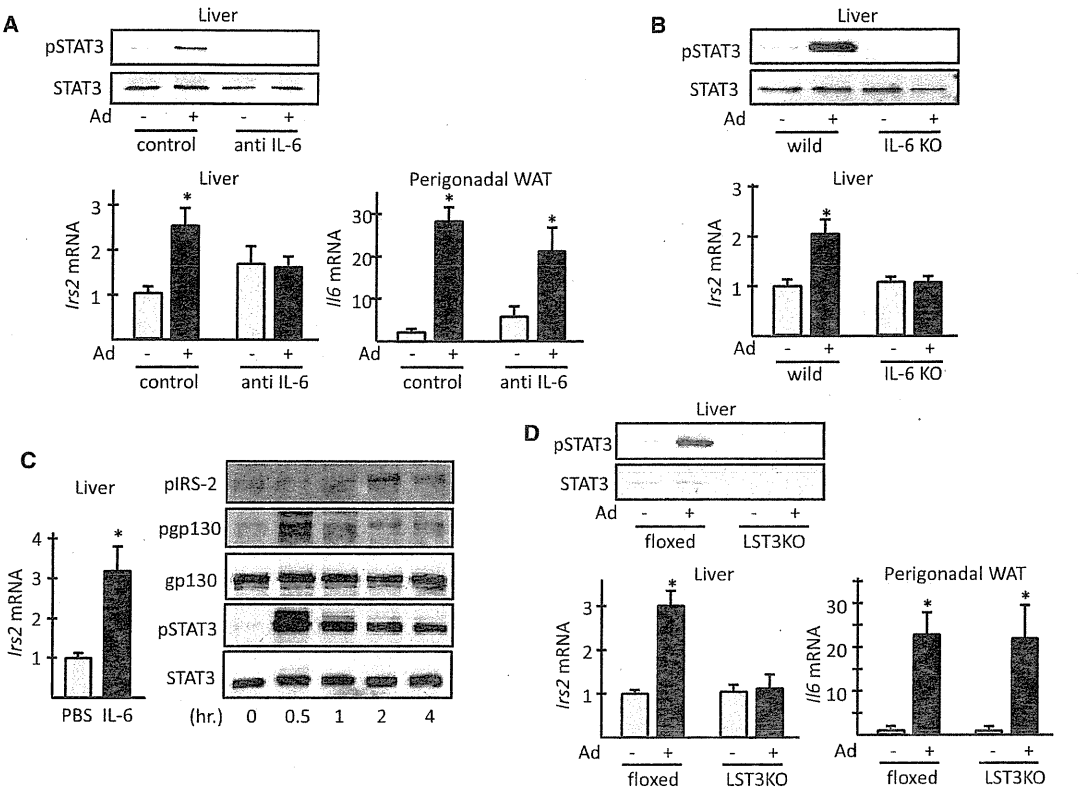

Figure 4. IL-6/STAT3 Signaling and Hepatic IRS-2 Upregulation by Adiponectin

(A) STAT3 signaling and IRS-2 induction with anti-IL6 antibody pretreatment. C57BL/6J mice pretreated with anti-IL6 antibody as described in the Experimental Procedures were injected with adiponectin (Ad) intraperitoneally, and the livers and perigonadal WAT were removed at 2 hr. The lysates of the livers were subjected to immunoblotting with pSTAT3/STAT3 antibody. The total mRNA was subjected to RT-PCR analysis for *Irs2* expression in liver and *Il6* expression in perigonadal WAT ($n = 5$, $^* p < 0.05$).

(B) STAT3 signaling and IRS-2 induction in IL-6 KO mice. IL-6KO mice and their control C57BL/6J (wild) mice were injected with Ad intraperitoneally, and the livers were removed at 2 hr. The lysates of the livers were subjected to immunoblotting with pSTAT3/STAT3 antibody. The total mRNA was subjected to RT-PCR analysis for *Irs2* expression in liver ($n = 5$, $^* p < 0.05$).

(C) STAT3 signaling and IRS-2 expression in liver after IL-6 administration. C57BL/6J mice were injected with recombinant human IL-6 intraperitoneally. The livers were removed at the indicated hours. The total mRNA extracted from the liver at 1 hr after IL-6 administration was subjected to RT-PCR analysis. The lysates of each liver sample were subjected to immunoprecipitation with the antibody for IRS-2, gp130, and STAT3, respectively, and subjected to immunoblotting with 4G10 anti-phosphotyrosine (for pIRS-2 and pgp130), gp130, pSTAT3, and STAT3 antibody as indicated ($n = 5$-6, $^* p < 0.05$).

(D) STAT3 signaling and IRS-2 induction in LST3KO. LST3KO or their control *flox/flox* mice (floxed) were injected with Ad intraperitoneally, and the livers and perigonadal WAT were removed at 2 hr. The lysates of the livers were subjected to immunoblotting with pSTAT3/STAT3 antibody. The total mRNA was subjected to RT-PCR analysis for *Irs2* expression in liver and *Il6* expression in perigonadal WAT ($n = 4$-6, $^* p < 0.05$).

Error bars represent mean ± SEM.

STAT3 and gp130 at 0.5 hr. The maximal *Irs2* mRNA upregulation after IL-6 administration occurred at 0.5–1 hr (data not shown), whereas the maximal STAT3 phosphorylation and *Irs2* upregulation after adiponectin administration occurred at 2 hr, further supporting that adiponectin secondarily upregulated IRS-2 via IL-6 induction.

Next, we administered adiponectin to mice with targeted disruption of STAT3 specifically in hepatocytes (LST3KO). In the livers of LST3KO mice, adiponectin-induced STAT3 phosphorylation and *Irs2* upregulation were totally abolished, while *Il6* induction by adiponectin was similar to that seen in the control *flox/flox* mice (Figure 4D). Collectively, these data indicated that adiponectin upregulated IRS-2 through STAT3 activation in hepatocytes in an IL-6-dependent manner.

Adiponectin-Induced IRS-2 Upregulation Was Mediated by STAT3 Recruitment to *Irs2* Promoter in Hepatocytes

Next, we focused on IRS-2 regulation by STAT3. Adenoviral-mediated overexpression of a constitutively active form of STAT3 (CA-STAT3) significantly increased IRS-2 in Fao cells (Figure 5A). Luciferase assay showed that wild-type (WT) or CA-STAT3 overexpression robustly enhanced *Irs2* promoter activity of the −1300 bps region, while the induction was diminished in the promoter deleted up to −500 bps (Figure 5B). The promoter region from −500 to −1300 bps contains multiple potential STAT3 binding sites. Indeed, chromatin immunoprecipitation (ChIP) assay in vivo confirmed that immunoprecipitation with STAT3 antibody significantly enriched the *Irs2* promoter regions in the livers at 1 and 2 hr after adiponectin administration,